THESIS FOR THE DEGREE OF DOCTOR OF PHILOSOPHY IN THERMO AND FLUID DYNAMICS

Analysis of concepts to reduce the environmental impact of aviation

High propulsive efficiency engines and contrail avoidance

LINDA LARSSON

Department of Applied Mechanics
CHALMERS UNIVERSITY OF TECHNOLOGY

Gothenburg, Sweden 2014

Analysis of concepts to reduce the environmental impact of aviation
High propulsive efficiency engines and contrail avoidance
LINDA LARSSON
ISBN 978-91-7597-000-4

Doktorsavhandlingar vid Chalmers tekniska högskola
Ny serie nr. 3681
ISSN 0346-718X
Department of Applied Mechanics
Chalmers University of Technology
SE-412 96 Gothenburg
Sweden
Telephone: +46 (0)31-772 1000

Chalmers Reproservice
Gothenburg, Sweden 2014

Analysis of concepts to reduce the environmental impact of aviation
High propulsive efficiency engines and contrail avoidance
Thesis for the degree of Doctor of Philosophy in Thermo and Fluid Dynamics
LINDA LARSSON
Department of Applied Mechanics
Chalmers University of Technology

Abstract

The average yearly increase in passenger kilometres travelled by air has been 5.8 % over the last 40 years. Fortunately the fuel consumption has not increased at the same rate. Over the same time period the average increase in fuel sold has been 2.2 % per year. However, if the growth of air traffic is going continue at the same pace, to minimise the climate effect, the rate of technological and operational improvement will have to increase.

In this thesis some options on how to reduce the climate impact of aviation have been analysed. A number of engine concepts to increase propulsive efficiency have been evaluated. The studies include a comparison between a geared turbofan and a two shaft direct drive turbofan for a future single aisle aircraft. Results show that the geared turbofan engine has a potential to reach approximately 4 % lower fuel consumption than a direct drive configuration.

Three options for the propulsion of a future regional aircraft have been analysed; an open rotor, an advanced turboprop and a turbofan engine. The specific range for this aircraft with varying Mach number for the three different engine options is shown. It is seen that the open rotor configuration combines low fuel consumption with the possibility of cruise Mach numbers normally associated with regional jets.

The thesis also includes analysis of the effect on fuel consumption when flying to reduce formation of persistent contrails. Data from real transatlantic flights have been used in this evaluation and the results show a less than 0.4 % increase in fuel consumption while reducing contrail formation by approximately 50 %.

The work has been carried out using a set of conceptual design tools to model engine performance, engine dimensions and weight, nacelle drag, aircraft performance and weight, as well as aircraft mission calculations. In the course of this work a number of sub models have been refined and some models have been added.

Keywords: Aviation, Environment, Aircraft engine, Open rotor, Turbofan, Turboprop, Contrails

List of publications

This thesis is based on the work contained within the following publications:

I L. Larsson, R. Avellán and T. Grönstedt, "Mission Optimization of the Geared Turbofan Engine", *20th ISABE Conferance*, September 12-16, Gothenburg, Sweden, ISABE-2011-1314, 2011

II L. Larsson, A. Lundbladh and T. Grönstedt, "Effects of different propeller models on open rotor fuel consumption", *21st ISABE Conferance*, September 9-13, Busan, South Korea, ISABE-2013-1712, 2013

III A. Lundbladh, L. Larsson and T. Grönstedt, "Transforming propulsion installation for commercial aircraft", *21st ISABE Conferance*, September 9-13, Busan, South Korea, ISABE-2013-1434, 2013

IV L. Larsson, A. Lundbladh and T. Grönstedt, "A conceptual design study of an open rotor powered regional aircraft",

Accepted for publication in ASME Turbo Expo 2014

V L. Larsson, D. Mitchell, T. Mårtensson and T. Grönstedt, "Effect on aircraft CO_2 emissions when flying to avoid the formation of persistent contrails -Based on continuous in-flight humidity measurements".

Submitted for publication in The Scientific World Journal

Other relevant publications:

- L. Larsson, T. Grönstedt and K.G. Kyprianidis, "Conceptual Design and Mission Analysis for a Geared Turbofan and an Open Rotor Configuration", *Proceedings of ASME Turbo Expo 2011*, June 6-10, Vancouver, Canada, 2011

Acknowledgements

This work was funded by the National Aviation Engineering Research Programme (NFFP) lead by the Swedish Armed Forces, the Swedish Defence Materiel Administration and the Swedish Governmental Agency for Innovation Systems. The work was carried out at the Department of Applied Mechanics, Division of Fluid Dynamics, at Chalmers University of Technology in collaboration with GKN Aerospace.

I would like to thank my supervisor Tomas Grönstedt for all the support throughout this work. With his patience and attention to detail it was possible to raise the quality of the work to the current level. Also, it would have been impossible to come this far without his expertise and speed in problem solving related to programming.

I am very grateful to my co-supervisor and colleague Anders Lundbladh at GKN Aerospace for all the discussions and for his ability to ask the difficult questions. I am also grateful to Richard Avellán for making it easy for me to continue work on the foundation he built.

A big thank you to all my colleagues and friends at Chalmers. You have made my time here more than just work. A special thank you to Deborah Rushton, it was a pleasure working with you. To bad we did not have time to do more projects together.

To all my colleagues at GKN Aerospace, thank you for a warm and friendly working environment and for making me feel at home. I look forward to working full time with you again.

Finally, I would like to thank all my friends and family for their support. A special thank you to Stefan who is always there for me, no mater what.

The trouble with the world is that the stupid are cocksure and the intelligent are full of doubt.
-Bertrand Russell

Nomenclature

A_0	Stream tube area far upstream
A_i	Nacelle inlet area
ATM	Air Traffic Management
BPR	Bypass Ratio
$CAEP$	Committee on Aviation Environmental Protection
CO_2	Carbon Dioxide
C_D	Coefficient of Drag
C_f	Coefficient of Thrust
C_L	Coefficient of Lift
C_p	Coefficient of Power
D	Propeller Diameter
D	Aircraft Drag
D_0	Stream tube diameter far upstream
D_{fan}	Fan diameter
D_i	Nacelle inlet diameter
D_m	Nacelle maximum diameter
$DDTF$	Direct Drive TurboFan
DL	Disc Loading
ETS	Emissions Trading System
F	Thrust
FPR	Fan Pressure Ratio
GDP	Gross Domestic Product
GTF	Geared Turbofan engine
GWP	Global Warming Potential
HPC	High Pressure Compressor
HPT	High Pressure Turbine
htr	Hub tip ratio
$ICAO$	International Civil Aviation Organisation
IPC	Intermediate Pressure Compressor
$ISSR$	Ice SuperSaturated Region
J	Advance ratio
L	Lift
L_a	Length of nacelle aftbody
L_c	Length of nacelle centerbody
L_f	Length of nacelle forebody
LPT	Low Pressure Turbine
M_{dr}	Drag rise Mach number
$\dot{m}$	Engine mass flow
$\dot{m}_0$	Inlet mass flow
$\dot{m}_9$	Outlet mass flow
$\dot{m}_f$	Fuel flow
MBM	Market Based Measure
n	Rotational speed

$NASA$	National Aviation and Space Agency
NO_x	Nitrogen oxides
OPR	Overall Pressure Ratio
P	Power
PR	Pressure Ratio
RHi	Relative Humidity over ice
RPK	Revenue Passenger Kilometer
S	Wing area
SFC	Specific Fuel Consumption
SR	Specific Range
$T3$	HPC outlet temperature
$T4$	Combustor outlet temperature
$T41$	HPT rotor inlet temperature
U	Blade speed
U_{tip}	Blade tip speed
UDF	UnDucted Fan
V_0	Aircraft velocity
V_9	Exhaust velocity
v_{18}/v_8	Bypass jet velocity over core jet velocity
W	Aircraft Weight
$W25$	HPC inlet mass flow
Q_f	Fuel Heating Value
Δh	Enthalpy change
η_o	Overall Efficiency
η_p	Propulsive Efficiency
$\eta_{propeller}$	Propeller Efficiency
η_{th}	Thermal Efficiency
η_{tm}	Propeller Efficiency divided by Propulsive Efficiency
ψ	Stage Loading
ρ	Density
Θ	Swirl angle

Contents

1 Introduction

1.1 Air transportation

In our society we take flying for granted. We go for vacation, business trips and we visit friends all over the world. However, travelling long distances is still a luxury that can not be afforded by everyone. There is a strong connection between GDP per person in a country and the average distance travelled. Schafer [1] shows that the time an average person spends travelling is fairly constant over time and largely independent of income level. It is shown that the major variation between different income levels is the distance travelled. The kilometres travelled are proportional to GDP. This means that when the GDP is growing, transportation moves towards higher speed transportation, such as high-speed trains and aircraft. This is why the distance increases while the time budget for travelling remains fairly constant.

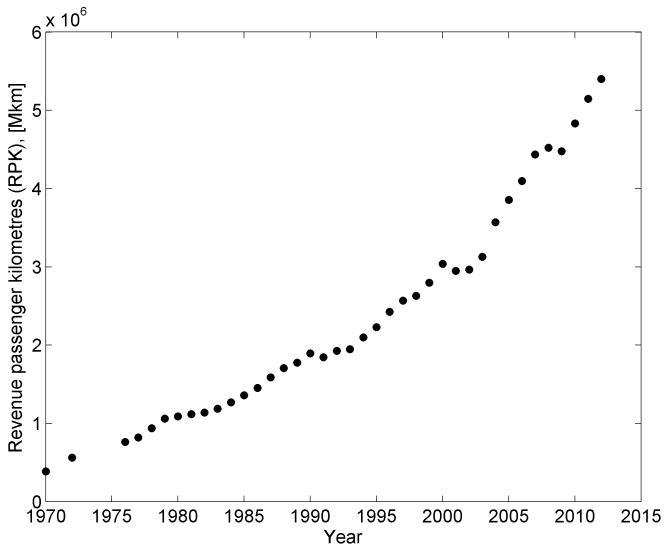

Figure 1.1.1: *World revenue passenger kilometres flown each year since 1970. Data is compiled from ICAO annual reports [2].*

In Figure 1.1.1 we look closer at the part of transportation that consists of travel by passenger aircraft. The total number of revenue passenger kilometres (RPK) travelled in the world is plotted against year. RPK is defined as the number of paying passengers multiplied by kilometres travelled. It can be seen that over the last 40 years there has been almost a tenfold increase in kilometres travelled worldwide.

Figure 1.1.2a shows the development of passenger kilometres for the airlines in four

different countries; China, India, the US and the UK. The United States clearly dominates the market and there has been a steady increase in passenger kilometres over time, but since 2006 the rate of increase is decreasing. The same is true for the United Kingdom. The major contribution to the increase in total passenger traffic is from China. China is the country with the world's largest population, followed by India. The development in these countries is therefore of high importance to the total growth of aviation. Figure 1.1.2b shows the average distance flown per inhabitant in the same four countries plotted against GDP per capita. For each country the development over time is shown. With increasing GDP the number of kilometres travelled has been increasing close to linearly.

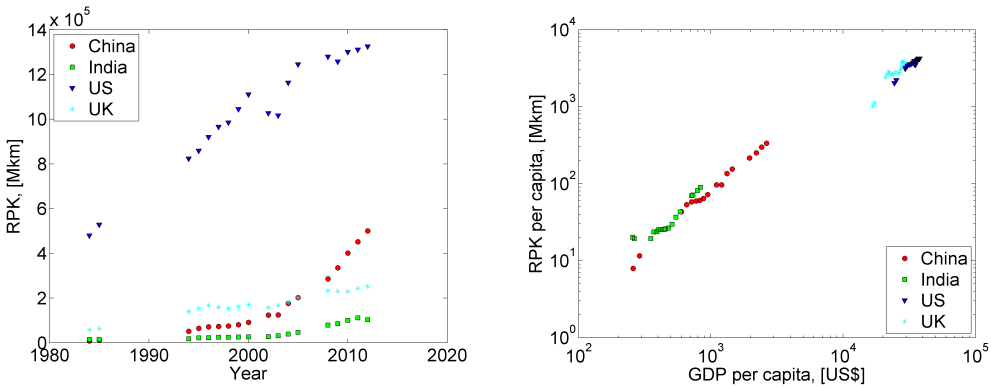

(a) *Per year* (b) *Per capita vs. GDP per capita*

Figure 1.1.2: *Revenue passenger kilometres for selected countries. Data is compiled from [2] and [3].*

Fortunately the growth of CO_2 emissions from aviation is not as large as the increase in passenger kilometres. In Figure 1.1.3 the relative change in aviation fuel sold together with passenger kilometres can be seen. Since 1972 the average yearly growth of revenue passenger kilometres has been 5.8 % while the average increase in aviation fuel sold has been 2.2 % per year. Although, it must be noted that the numbers for aviation fuel sold includes fuel used for cargo and military. This means that the two curves are not entirely comparable.

There are a number of reasons why the fuel consumption has not increased at the same rate as the passenger kilometres. One is that the load factor of the aircraft has increased. In 2012, according to ICAO, 79 % of the seats were occupied compared to 67 % in 1994. Another factor is that there has been significant improvements in aircraft performance over the years an shown by Avellán [4]. Still, if the growth of air traffic is going continue at the same pace, to minimise the climate effects, the rate of technological and operational improvement will have to increase and renewable fuels will have to be used.

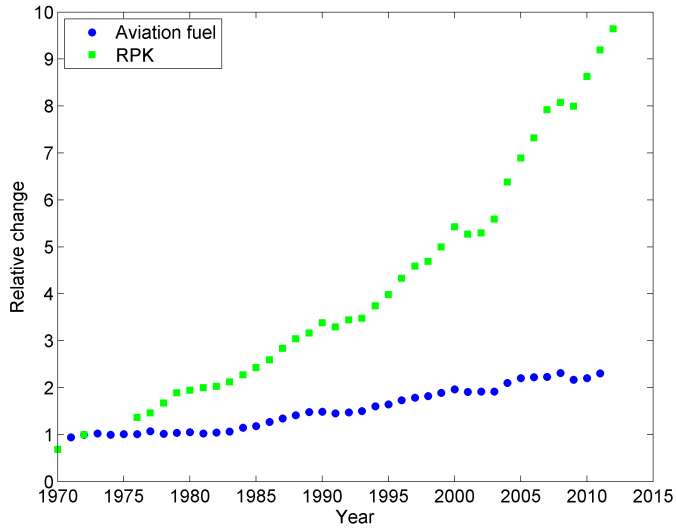

Figure 1.1.3: *Relative change in passenger kilometres and in aviation fuel sold. [2, 5]*

1.2 Climate effects of aviation

Aviation has several different effects on the earth's climate. Firstly there is the effect of carbon dioxide (CO_2) emissions. The effect of CO_2 on the climate is relatively well known [6]. It has the same impact regardless of whether it is emitted on the ground or at high altitude. This is the gas we normally associate with greenhouse gases. The other two major climate effects come from NO_x and water.

Different types of nitrogen oxides, or NO_x, chemically react with greenhouse gases in the atmosphere. Depending on which reaction occurs, the contribution to global warming differs. It contributes to the production of tropospheric ozone which has a warming effect. NO_x also reacts with methane and breaks it down. Since methane is a strong greenhouse gas the reaction between NO_x and methane has a cooling effect. Whether NO_x has a cooling or warming effect, and what the magnitude of this effect is depends on when and where NO_x is emitted. The reactions are different for different altitudes, latitudes and seasons. The climate impact of NO_x varies with how much time has passed since the emission occurred. This is because the residence time in the atmosphere is limited and also because different reactions occur at different times.

A third climate effect is from water in the atmosphere, especially from the formation of condensation trails or contrails. Contrails form when humid air condenses to ice crystals. They are a form of aviation induced high altitude clouds, so called cirrus clouds. Contrails reduce the incoming solar radiation and reduce the heat leaving earth [7]. Thus the contrails can be both warming and cooling depending on time of day and season.

If contrails are formed or not is largely dependent on the ambient relative humidity.

Figure 1.2.1: *Condensation trails*

Since contrails are ice clouds it is the relative humidity over ice (RHi) that is of interest, ie. if the air is ice super saturated or not. When RHi is below 100 % no persistent contrails are formed. Any contrails formed in low humidity air rapidly evaporate. When the relative humidity over ice is between 140-160 % cirrus clouds are formed naturally. In the region in between 100-140 % RHi there is a risk of formation of clouds where otherwise no cirrus clouds would have occurred [8].

In the exhaust plume behind the engine the humidity is locally higher due to water formation in the combustion of hydrocarbons. When this humid air is mixed with the cooler ambient air water condenses into droplets. When these droplets freeze in the cold air they can act as nuclei in the condensation of the ice super saturated air in the surroundings. In that case the contrail grows and is persistent. Other emissions, such as soot or small volatile particles, can also act as nuclei in the condensation [7, 8].

One of the largest uncertainties is to what extent persistent contrails transform and add to the formation of cirrus clouds. If a cirrus cloud is observed where earlier there was a contrail, it is not known if it stemmed from the contrail, or if it would have occurred naturally.

1.2.1 Magnitude

One measure often used in the context of global warming is radiative forcing. This is a measure of how the radiation balance on earth is perturbed by the presence of an emitted substance. In Penner et al. [9] the radiative forcing in 1992 caused by aviation is calculated. The numbers show a snapshot of the radiative forcing caused by all historical aviation up to 1992. Later updates have been made and can be seen for 2000 in Sausen et al. [6] and for 2005 in Lee et al. [10]. In the two latter references the numbers differ from those in 1992 partly due to more refined models but also due to the effects of increased air traffic. In Lee et al. [10] the radiative forcing from aviation is presented to be 0.055 W/m^2, not including the effect of cirrus clouds.

The ozone produced due to NO_x causes radiative forcing approximately in the same order of magnitude as CO_2, but since there also is a negative radiative forcing due to destruction of methane the total contribution from NO_x is around 1/4 of the total aviation induced radiative forcing. Around 1/5 of the total radiative forcing is due to formation of linear contrails. The numbers above do not take into consideration the effect of induced cirrus clouds. The magnitude of this effect is very uncertain; the best estimate at this point according to Lee et al. [10] is 0.033 W/m^2. The calculation of how much contrail formation contribute to aviation induced radiative forcing is highly sensitive to modelling and thus the uncertainties are large. This is exemplified in the recent paper by Chen and Gettelman [11] where the total contribution to global radiative forcing by linear contrails and contrail cirrus is calculated to be approximately 1/3 of the radiative forcing calculated by Lee et al. [10].

Radiative forcing is a steady state figure of the current effect on global warming. There are different measures to account for the variation over time and for the different time scales involved. Global warming potential (GWP) is the integration of radiative forcing over a given time. The time horizon integrated over is of great importance. CO_2, for example, has an effect on the climate for several hundreds of years, whilst NO_x and contrails only have an effect over a shorter time span. When calculating the GWP (without the effect of induced cloudiness) with a 20 year time horizon, the total contribution is between 2.1 and 2.6 times that of the contribution from CO_2 only [10]. When performing the same integration for a 100 year horizon the corresponding values are between 1.3 and 1.4. It is also difficult to reflect in the calculations that while the effect of CO_2 is global, NO_x and contrails affect the climate on a relatively local scale.

The figures discussed above are historical numbers for global aviation until the present day. It is important that these numbers are not interpreted as a factor to multiply the CO_2 emissions by to get the climate effect of a single flight. When evaluating different engine and aircraft technologies and mission profiles a more precise measure is needed. Just because the average contribution of aviation to global warming so far has been two times that of CO_2 only (depending on measure), it does not mean that it will be so in the future. More importantly, it will not be the same for every flight. If, for example, the flight level is reduced to avoid the generation of contrails on a certain day, the CO_2 emissions might increase due to increased aircraft drag, but the climate effect in total decreases. There are differences depending on type of flight as well. Karyd [12] mentions in his report that generally the domestic flights of Sweden only affect the climate by its

CO_2 emissions, since most of the flights are short and do not reach altitudes where there is a negative influence from contrails and NO_x emissions.

1.3 Economical incentives

Political discussions on how to provide economic incentives to reduce global warming from aviation is on going. Should there be a global tax on aviation fuel or are there other solutions? Should only CO_2 be included in the scheme, or should it also include the climate effects of other types of emissions?

Since 2012 all EU-flights are included in the European Emissions Trading System (ETS)[13]. Although, flights to and from EU were for 2012 temporarily exempted to allow time for ICAO to reach a global agreement on measures to control CO_2 emissions. In October 2013 [14] it was agreed to propose a global market-based measure (MBM) to reduce the growth of aviation induced CO_2 emissions. The proposal shall be presented in 2016 be ready for implementation by 2020. The current proposal (at the time of writing) by the EU Commission is to only include the portion of flights that takes place within European airspace in the ETS [15, 16, 17]. Thus it appears that a global agreement on economic incentives to reduce climate effects of aviation will at earliest be implemented in 2020.

There has also been a decision at the 9th Committee on Aviation Environmental Protection (CAEP) meeting to include CO_2 emissions in the certification of new aircraft [18]. The CO_2 certification standard will complement the already existing noise and emission certification requirements.

1.4 Scope of thesis

In this thesis ways to reduce the climate impact of aviation have been analysed and evaluated. The first part is focused on analysing and evaluating different engine concepts for high propulsive efficiency in order to reduce aircraft fuel consumption and thereby reduce CO_2 emissions. The second part evaluates the effect on fuel consumption when flying to reduce formation of persistent contrails.

The work has been carried out with a set of tools both commercially available and tools developed at Chalmers. In the course of this work a number of sub models have been refined and some models have been added.

Chapter 1 of the thesis gives some background to why this work is important. Basic figures of merit that are important in the evaluation of aircraft and engines are introduced in Chapter 2. In Chapter 3 the methods used in the calculations are presented. In Chapter 4 and 5 some concepts on high propulsive efficiency engines are evaluated on short to medium range aircraft. The effect on fuel consumption when flying to reduce formation of persistent contrails during transatlantic flights is discussed in Chapter 6. Division of work and comments to the appended papers can be seen in Chapter 7 and concluding remarks in Chapter 8.

The work has been carried out in collaboration between GKN Aerospace and Chalmers.

2 Engine and aircraft performance

When evaluating the benefits of different aircraft and engine configurations several figures of merit such as efficiency, specific fuel consumption and specific range can be calculated. In this chapter selected concepts central to the understanding of aircraft and engine performance are presented.

2.1 Engine performance

The purpose of the engine is to provide thrust to propel the aircraft. For a fully expanded flow (when neglecting the fuel flow) the thrust (F) is given by the difference in velocity between the exhaust jet (V_9) and the aircraft flight speed (V_0) multiplied by the mass flow, $\dot{m}$ (Eq. 2.1.1). This relationship can be derived from the momentum equation.

$$F = \dot{m}(V_9 - V_0) \tag{2.1.1}$$

How efficiently the thrust is produced can be seen from specific fuel consumption (Eq. 2.1.2). SFC is the fuel flow ($\dot{m}_f$) needed per unit of thrust produced.

$$SFC = \frac{\dot{m}_f}{F} \tag{2.1.2}$$

The overall efficiency of the engine is the power propelling the aircraft (thrust times flight speed), divided by the thermal power (fuel flow times fuel heating value, Q_f) available within the fuel (Eq. 2.1.3). Thus it is a measure of how efficiently the available energy within the fuel is used to propel the aircraft.

$$\eta_0 = \frac{F \cdot V_0}{\dot{m}_f Q_f} = \frac{V_0}{SFC \times Q_f} = \eta_p \eta_{th} \tag{2.1.3}$$

The overall efficiency can be divided into thermal efficiency, η_{th} (Eq. 2.1.4) and propulsive efficiency, η_p (Eq. 2.1.5). The thermal efficiency shows how well the energy within the fuel is transformed into kinetic energy available to produce thrust. Propulsive efficiency shows how well the available kinetic energy is used to produce thrust. High propulsive efficiency is achieved when the difference between the flight speed and exhaust velocity is small. As is seen in Equation 2.1.1, with a high propulsive efficiency, a high mass flow is needed in order to produce required thrust.

$$\eta_{th} = \frac{\dot{m}_9 \frac{V_9^2}{2} - \dot{m}_0 \frac{V_0^2}{2}}{\dot{m}_f \; Q_f} \tag{2.1.4}$$

$$\eta_p = \frac{F \cdot V_0}{\dot{m}_9 \frac{V_9^2}{2} - \dot{m}_0 \frac{V_0^2}{2}} \approx \frac{2}{1 + \frac{V_9}{V_0}} \tag{2.1.5}$$

When calculating the dimensions and weight of turbomachinery one important dimensionless number is stage loading, ψ (Eq. 2.1.6). It is the enthalpy change (Δh) over a compressor or turbine stage divided by the blade speed (U) squared (often mid radius

blade speed). The allowable stage loading together with annulus dimensions and rotational speed govern the number of turbo machinery stages needed.

$$\psi = \frac{\Delta h}{U^2} \tag{2.1.6}$$

2.2 Propeller performance

In this thesis open rotor engines and turboprops are discussed, therefore an overview of propeller performance is relevant. Propeller efficiency is often presented in propeller maps as a function of the two dimensionless numbers; advance ratio, J (Eq. 2.2.1) and coefficient of power, C_p (Eq. 2.2.2). Advance ratio is the speed with which the propeller moves forward in the air relative to the rotational speed of the propeller, ie. flight velocity divided by rotational speed (n) times propeller diameter (D).

$$J = \frac{V_0}{nD} \tag{2.2.1}$$

$$C_p = \frac{P}{\rho n^3 D^5} \tag{2.2.2}$$

The propeller efficiency (Eq. 2.2.3) relates the available shaft power (P) to the useful thrust produced by the propeller. The efficiency can be expressed as a relationship between thrust and power, and also between the coefficient of power and the coefficient of thrust (Eq. 2.2.4).

$$\eta_{propeller} = \frac{F\ V_0}{P} = \frac{C_f\ J}{C_p} \tag{2.2.3}$$

$$C_f = \frac{F}{\rho n^2 D^4} \tag{2.2.4}$$

Propeller efficiency includes all the loss sources in the propeller, i.e. axial kinetic losses (propulsive efficiency), swirl losses as well as turbo machinery losses. If the propeller efficiency is divided by propulsive efficiency, the result is a measure of how well the propeller converts shaft power to kinetic energy (Eq. 2.2.5). This efficiency corresponds to the fan component efficiency in a conventional turbofan.

$$\eta_{tm} = \frac{\eta_{propeller}}{\eta_p} = \frac{\dot{m}_9 \frac{V_9^2}{2} - \dot{m}_0 \frac{V_0^2}{2}}{P} \tag{2.2.5}$$

Two of the parameters often used to find the desired design is propeller blade tip speed, U_{tip}, and disc loading, DL (Eq. 2.2.6).

$$DL = \frac{P}{D^2} \tag{2.2.6}$$

Propeller blade tip speed and advance ratio are related by Equation 2.2.7. Disc loading is related to advance ratio and power coefficient by Equation 2.2.8. As can be deduced

from the equations, when decreasing blade tip speed, the disc loading needs to be reduced if the same power coefficient is sought.

$$J = \frac{V_0 \pi}{U_{tip}} \tag{2.2.7}$$

$$C_p = DL \frac{J^3}{V_0^3 \rho} \tag{2.2.8}$$

2.3 Aircraft performance

As mentioned earlier the purpose of the engine is to provide the thrust the aircraft requires. For level flight, enough thrust is needed so that the weight (W) of the aircraft is balanced by the lift provided by the wings (Eq. 2.3.1). The thrust required is determined by the aerodynamic performance of the aircraft, which is often given as a ratio between lift and drag, L/D.

$$F = \frac{W}{L/D} \tag{2.3.1}$$

The lift coefficient, C_L (Eq. 2.3.2) is a dimensionless number relating the lift to the dynamic pressure and the wing area (S). A corresponding number for drag is the drag coefficient, C_D (Eq. 2.3.3). The magnitude of C_L and C_D depends on the geometry of the aircraft. For a specific aircraft the parameters vary with angle of attack, Mach number and flight altitude.

$$C_L = \frac{L}{\rho \frac{1}{2} V_0^2 S} \tag{2.3.2}$$

$$C_D = \frac{D}{\rho \frac{1}{2} V_0^2 S} \tag{2.3.3}$$

Specific range, SR (Eq. 2.3.4) is often used as a number to evaluate the efficiency of an aircraft. It is the distance the aircraft can travel per unit fuel mass. To calculate specific range the current speed of the aircraft, weight of the aircraft, aerodynamic performance (L/D) and specific fuel consumption is needed. For a good aircraft design a high L/D ratio, low aircraft weight and low specific fuel consumption is sought. All of these parameters vary throughout the mission. The specific range can be used to find the optimal flight speed and altitude for the current aircraft weight throughout the mission.

$$SR = \frac{V_0 \ L/D}{WSFC} \tag{2.3.4}$$

3 Methods

Within this thesis different engine options, aircraft configurations and aircraft trajectories have been evaluated, mainly in terms of fuel consumption. This requires tools to model engine performance, engine dimensions and weight, nacelle drag, aircraft performance and weight, as well as aircraft mission calculations. The tools have been used to both calculate the fuel consumption of existing aircraft and for conceptual design and evaluation of future aircraft/engine concepts. In this chapter the main tools used within this thesis are described.

3.1 Engine performance calculations

Engine performance calculations have been made using either the commercially available GasTurb 11 developed by Kurzke [19] or using the in-house tool GESTPAN largely developed by Grönstedt [20].

GESTPAN functionalities includes engine design performance calculations, off design calculations and mission analysis. It is a module based tool, with the possibility to build models of a wide range of engine configurations. Examples of modules that exist are compressor, turbine, propeller, intercooler and nacelle. New modules can be defined if needed. The modules are in the input file connected so that the output mass flow, temperature and pressure of an upstream component is given as input to the downstream component.

After the module components for the engines are chosen and the connections between the modules are made, some basic thermodynamic design parameters need to be set. For a turbofan engine these parameters include compressor pressure ratio, component efficiency, bypass ratio (BPR), combustor outlet temperature and engine mass flow. The required cooling flow to the high pressure turbine (HPT) is calculated using the method presented by Young and Wilcock et al. [21, 22] where a maximum allowable metal temperature is set and cooling flow efficiency parameters are chosen. The cooling flow requirement is calculated individually for each turbine stage.

GasTurb 11 is a tool to calculate design and off design engine performance. One difference between GasTurb and GESTPAN is that GasTurb has a set of pre defined engine configurations. The predefined configurations makes the process of setting up a working performance model very easy. The drawback is that the tool is not as flexible. As in GESTPAN some thermodynamic design parameters are required as input to the calculations. Output from the calculations can either be a thermodynamic overview of the engine at different operational points, or selected parameters exported for the aircraft operational envelope.

3.2 Engine dimensions and weight

Engine weight is modelled using the in-house code WEICO [23, 24] developed within the VITAL project by Grönstedt. The basis for the calculations come from the method

presented by Onat and Klees [25].

Within the code the dimensions and weight of each engine component is calculated. For the compressors and turbines the dimensions of the annulus is given by pressure, temperature and mass flow at the inlet and outlet of each component. Many parameters are either set as input data or calculated. These parameters include for example inlet and outlet axial Mach number, blade tip speed, allowed maximum stage loading, number of stages, deHaller number, hub tip ratio, blade aspect ratio and geometrical constraints from other components. It is possible to chose which of these parameters are to be calculated and which of them are set.

After the annulus is set the number of blades in each blade row is decided by the defined solidity. The height and width of the blade together with a volume factor give a blade volume for which a weight can be calculated. The blade weight together with the rotational speed is used as input to the calculation of the disc stress and weight. Weight of the casing is calculated using containment requirements and dimensions.

The engine weight also includes weight of structures, which are calculated with for example number of struts and dimensions as input. Shaft weight is estimated based on torque. The nacelle weight is calculated from the geometry of the nacelle and includes weight of inlet, cowl and support material.

When calculating the weight of the engine, close attention has to be paid to the modelling of the components contributing most to engine weight. It is in those components the choice of for example Mach numbers and stage loading matter the most. The final weight of the engine is highly dependent on the constraints on for example the low pressure turbine, choice of fan blade aspect ratio and on chosen nacelle length. For conceptual design of future engines relevant input data can be chosen by looking at trends in existing engines. Many such trends are presented by Greib in [26].

3.3 Nacelle drag

Nacelle drag can be calculated either in GISMO (described in the next section) or GESTPAN and is based on the method presented in an ESDU report [27]. Within this method the nacelle drag is divided into three components; profile drag, spillage drag and wave drag. Spillage drag occurs when the flow separates around the nacelle forebody. This occurs when the nacelle has a flow capacity much larger than required for the current flight conditions. Wave drag occurs when the flow around the nacelle at some point accelerates to Mach numbers above one. The profile drag is the drag caused by friction and pressure drag.

The magnitude of the different contributors to drag depends on the nacelle geometry and on the flight conditions. The main geometrical inputs used are shown in Figure 3.3.1. The parameters are: length of nacelle forebody (L_f) in relation to fan diameter (D_{fan}); the inlet diameter (D_i), in relation to D_{fan} and nacelle maximum diameter (D_m) in relation to D_{fan}.

From the known flight Mach number, ambient temperature, pressure and density together with the engine mass flow the stream tube area (illustrated by diameter D_0) far upstream from the engine, the nacelle drag coefficient can be calculated.

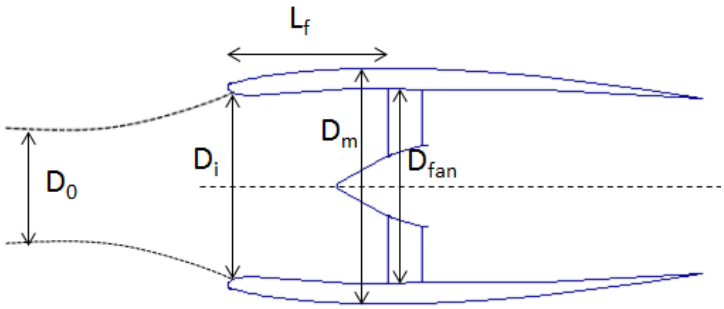

Figure 3.3.1: *Schematic drawing of a nacelle, with main geometrical parameters indicated*

Based on the input parameters it is determined if there is spill drag and wave drag. For the nacelle there is a critical area ratio between the inlet area (A_i) and the upstream stream tube area (A_0). If the ratio $\frac{A_0}{A_i}$ is below this critical value there will be spillage drag. The critical area ratio is modelled using the length of the inlet and the difference between D_i and D_m. For a short inlet and a thick nacelle the critical area ratio will be small and the flow will not separate at the inlet as easily.

The occurrence of wave drag is determined by finding the critical drag rise Mach number, M_{dr}. If the free stream velocity exceeds M_{dr} there will be wave drag. A short inlet together with a large difference between D_i and D_m yields a low M_{dr}. To have a high M_{dr} the nacelle forebody needs to be long and slender. The existence of spillage drag will reduce the critical Mach number.

It is the same geometrical parameters that determine the critical area ratio and the drag rise Mach number. A long and slender inlet is beneficial for wave drag, while a short and thick inlet is beneficial for the spillage drag.

The profile drag coefficient is found from the flat plate skin friction multiplied with a form factor. The magnitude of the form factor depends on the form of the forebody (L_f), afterbody (L_a) and the length of the cylindrical midbody (L_c). It also depends on the stream tube area ratio.

The drag coefficients from profile drag, spillage drag and wave drag are calculated and added. The total nacelle drag is then found with the maximum frontal projected area of the nacelle as reference area.

3.4 Aircraft calculations

Aircraft performance, weight and dimensions are calculated using the in-house code GISMO developed by Avellán [4, 28]. The geometry and weight of the aircraft is calculated using methods described by Torenbeek [29]. Most of the aerodynamic performance of the aircraft is calculated based on correlations presented by Roskam in [30].

Firstly the aircraft geometry is calculated. The fuselage cross section is determined by the chosen seat and class configuration. The length of the aircraft is then determined by

the number of seats together with for example the required number of galleys, toilets and doors. The wing geometry is defined by the sweep angle at 1/3 chord length, wing area, wing aspect ratio and wing taper ratio. Other geometry input such as tail sweep, tail and nose fineness are also used.

After the geometry of the aircraft is determined the weight of the aircraft is calculated. The fuselage weight is calculated based on the wetted area of the fuselage, with additional weight for for example, doors, hatches, floor and so on. The wing weight is calculated so that the structure can withstand maximum bending moment at its design speed in the event of a strong gust. Weight of for example landing gear, control surfaces and operational items are also calculated.

Finally the aerodynamic performance in terms of lift and drag for different angles of attack is calculated. The wing lift coefficient is calculated using the relations from Roskam [30]. The coefficients of drag for the fuselage, empennage, pylon, nacelle wind shield and flaps are then calculated. The lift and drag coefficient varies with varying altitude and Mach number.

3.5 Propeller performance

In order to calculate performance of counter-rotating open rotor engines a method to represent the counter-rotating propeller is needed. In Paper II such a method is presented.

It is convenient to describe propeller performance in the form of propeller maps with the efficiency as a function of advance ratio and power coefficient. For counter-rotating propeller there is no such extensive dataset available in the public domain. Therefore, a map for an advanced single-rotating propeller was used as a basis to find a map for a counter-rotating propeller. This map is found in [31]. The data set covers a large range of power coefficients and advance ratios as well as Mach numbers. The original maps for low Mach numbers and for Mach 0.8 are shown in Figure 3.5.1.

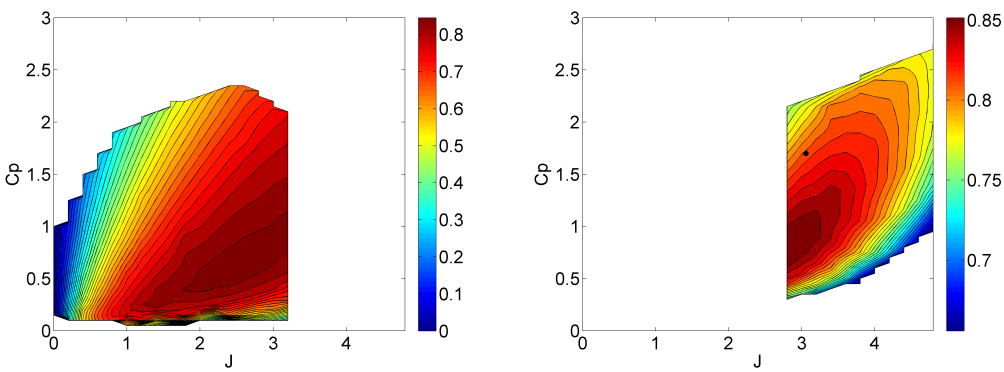

(a) *Low Mach numbers* (b) *Mach 0.8*

Figure 3.5.1: *Maps for an advanced single-rotating propeller [31]*

The losses contributing to total propeller efficiency includes swirl losses, turbomachinery losses (profile losses, shock losses) and axial kinetic losses (propulsive efficiency). The main differences between a single-rotating propeller and a counter-rotating propeller is that most of the swirl generated in the front propeller stage is recovered in the rear stage. Since there are two stages, more power per disc area is possible.

The swirl losses and propulsive efficiency were calculated using the slip stream data provided with the propeller maps. Equation 3.5.1 and Equation 3.5.2 give the swirl losses and propulsive efficiency. The derivation of the equations can be found in Paper II. The swirl losses found are shown in Figure 3.5.2a and the propulsive efficiency for Mach 0.8 is shown in Figure 3.5.2b. Equation 3.5.2 is derived from actuator disc theory. Note that if compressible actuator disc theory [32] is used the resulting propulsive efficiency do not differ, only the velocities close to the propeller plane differs.

$$SwirlLoss = \frac{\pi(1 - htr^2)}{8} \frac{J^3(1 + \frac{\Delta v}{v_0})^3 \tan^2 \Theta}{C_p} \tag{3.5.1}$$

$$\eta_p = \frac{2}{1 + \sqrt{1 + \frac{C_f 8}{J^2 \pi(1 - htr^2)}}} \tag{3.5.2}$$

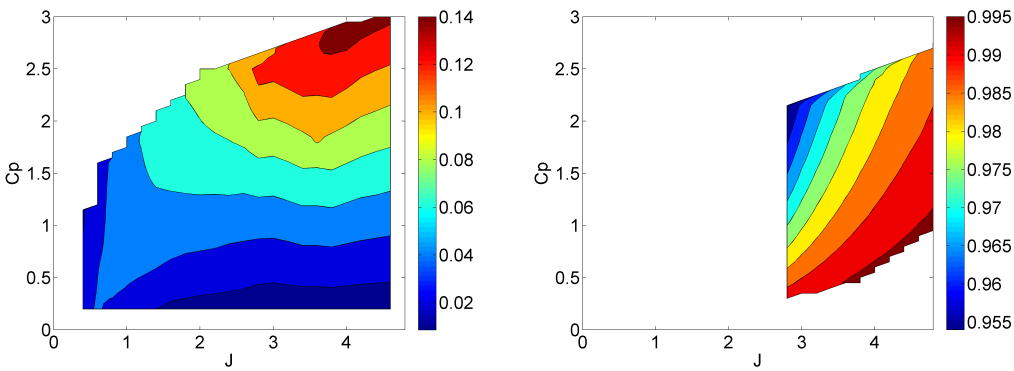

(a) *Swirl losses* (b) *Propulsive efficiency*

Figure 3.5.2: *The swirl losses and propulsive efficiency as calculated from the propeller data for a single-rotating propeller [31]*

To represent the counter-rotating propeller 90 % of the swirl losses are removed from the map. To represent a two stage propeller where more power per disc area is possible the scale of the C_p axis is changed.

The resulting propeller map is shown in Figure 3.5.3a. This can be compared to the map of the F7A7-propeller, a tested counter-rotating propeller [33] in Figure 3.5.3b. The resemblance of the topology is clear. The benefit with this map compared to the F7A7 map is that this covers a much larger operational range and thus can be used in a larger design space.

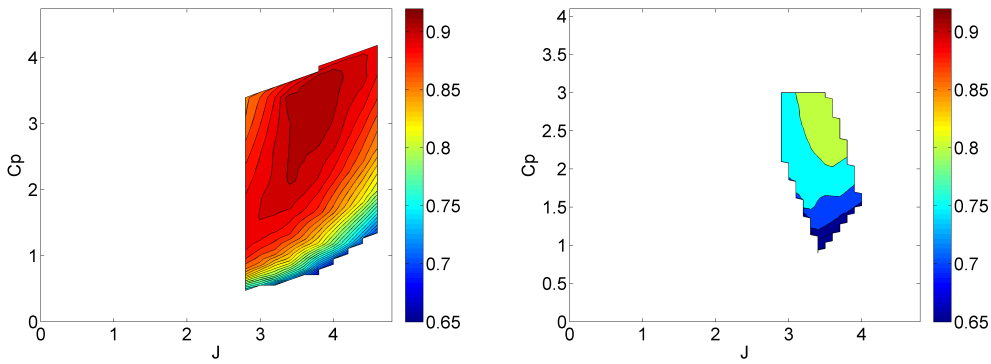

(a) *Propeller map for CR-propeller* (b) *F7A7*

Figure 3.5.3: *The resulting propeller map of a counter-rotating propeller together with the map derived from experimental data in [33]*

When using this method to calculate propeller performance the axial kinetic losses are removed from the map by dividing propeller efficiency with propulsive efficiency. The propulsive efficiency is then calculated separately in the performance calculations using actuator disc theory. This means that the maps can be scaled while still being able to capture the effect of disc loading on propulsive efficiency. The absolute magnitude of efficiencies can also be scaled in the map, as is done in Paper IV.

3.6 Mission analysis

With the knowledge of engine performance, aircraft lift and drag, engine and aircraft weight; calculations of an entire mission can be made. The goal of such studies can for example be to find the fuel consumption for an entire mission or to study how a trajectory change affects the fuel consumption.

In GESTPAN there is a mission optimization functionality. In the input file the parts of the mission are defined, such as take-off, initial climb, final climb and cruise. The different parts of the missions can have different constraints, for example max thrust, a certain climb gradient or a certain speed. As input C_L and C_D for different angles of attack are needed. After the aircraft engine design calculations are done and the weight of the engine is determined the mission optimization is started. Using for example Equation 2.3.1 the thrust required, aircraft angle of attack and climb gradient can be found. The fuel consumption for each time step of the mission is then calculated and the aircraft weight is updated to the next time step. After the entire mission has been calculated the total fuel consumption is found.

The engine performance for each step of the mission is calculated as the inlet conditions for the engine changes and the thrust requirements changes. Since the mission calculations are carried out directly within GESTPAN the engine design parameters can easily be optimized not only for minimal fuel SFC at one ore more design points but for a minimal

fuel consumption for the entire mission.

A similar method to calculate mission fuel consumption has been implemented in MATLAB and was used in the calculations presented in Paper V. Here, the engine performance was calculated using GasTurb 11. The thrust and SFC for different thrust settings were calculated and exported to tables; one table for each Mach number and altitude. The required thrust is found in the same manner as in GESTPAN. SFC for the required thrust and current flight conditions is found by interpolating between the tables. The fuel flow is then calculated and the aircraft mass is updated for the next time step. This MATLAB implementation does not only have to be used for mission calculation. A similar implementation was used in Paper IV to find the specific range at different altitudes, Mach numbers and for different aircraft weight.

4 High bypass ratio turbofan engines

Since the first commercial aircraft with jet engines were developed at the end of the 1950s, there have been many advances. One of the most significant changes has been the development of the turbofan engine. This type of engine enabled substantial improvements in fuel consumption compared to the single stream turbojet engine due to increased propulsive efficiency. Most modern civil aircraft today are equipped with turbofan engines.

Figure 4.0.1 shows a schematic illustration of a turbofan engine. Air enters the engine inlet and is compressed in the fan (1). After exiting the fan some of the air is lead directly to the exhaust nozzle where the velocity of the air increases and thrust is produced. The rest of the air enters the compressors (2) where the pressure and thus temperature is increased. In the combustor (3) fuel is added and combustion occurs which results in added thermal energy. The air then enters the turbines (4) where thermal energy is converted into shaft power to drive the compressors. The air then enters the nozzle where it expands and thrust is produced.

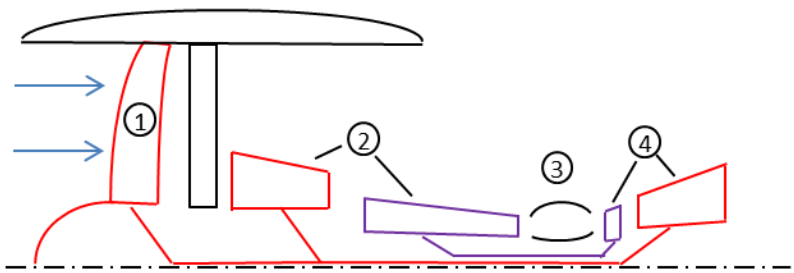

Figure 4.0.1: *Schematic figure of a turbofan engine*

To reach high propulsive efficiency in a turbofan engine the thrust needs to be produced with a small difference between flight velocity and engine exhaust air velocity. In modern turbofan engines the main part of the thrust is generated by air passing through the bypass channel. The rest of the thrust comes from the core mass flow. Guha [34] shows in his paper that minimum SFC is reached when there is a velocity ratio between the bypass jet and the core jet (v_{18}/v_8) in the order of 0.8. The optimal value depends on the low pressure turbine (LPT), fan and nozzle efficiency. In order to increase propulsive efficiency it is not enough to reduce the fan pressure giving lower bypass nozzle velocity. The velocity of the core nozzle flow also needs to be reduced. The lower core exhaust velocity is achieved by increasing the bypass ratio and extracting more work from the LPT. High propulsive efficiency turbofan engines have large fans to accommodate the large mass flows needed to produce required thrust. The high bypass ratio is a result of finding the optimal velocity split and does not in itself give low fuel consumption.

Although high propulsive efficiency is beneficial for the overall efficiency, it might not be beneficial for the total fuel consumption. Large fan diameter leads to heavy engines and high nacelle drag. For a turbofan engine there is a trade-off between propulsive efficiency and weight/drag. Also, as the pressure ratio over the fan decreases, the pressure losses in the bypass duct play a comparatively larger role.

For a two shaft turbofan engine the maximum allowable fan tip speed sets the rotational speed of the low pressure shaft. For high bypass ratio engines this means that the rotational speeds of the intermediate pressure compressor and low pressure turbine are relatively low. In order to keep the stage loading (as defined in Equation 2.1.6) at an acceptable level the blade speed needs to increase or the change in enthalpy (Δh) per stage needs to decrease. With a fixed rotational speed the blade speed can only be increased by increasing the radius of the turbine. Since it is not possible to extend the radius of the turbine indefinitely, the number of turbine stages will still have increase with increasing power demand.

One way to alleviate this problem is to introduce a reduction gear box between the fan and intermediate pressure compressor (IPC). This means that the turbine can rotate at a more optimal speed. The radius of the turbine can be reduced and the required power can be produced with significantly fewer stages. The design can be chosen so that the stage loading is lower than for a direct drive turbofan, and a higher LPT efficiency can be achieved. For the IPC the increased rotational speed means that a higher stage pressure ratio and a lower stage loading can be achieved. As a result higher IPC pressure ratio, fewer stages and increased efficiency is possible.

There are other limitations and constraints in aircraft engine design. To maximize thermal efficiency it is desirable to have an, as high as possible, overall pressure ratio (OPR) and combustor outlet temperature. The OPR is often limited by the minimum allowable blade hight for the last stage in the high pressure compressor (HPC). Blade heights below this limit would exhibit significant efficiency losses. The OPR might also be limited by the maximum allowable compressor metal temperature. The maximum combustor outlet temperature and the required cooling flow are determined by high pressure turbine material.

4.1 Comparison between a direct drive and a geared turbofan engine

In Paper I a study comparing a geared turbofan engine and a two shaft direct drive turbofan engine is presented. Bypass ratio and fan pressure ratio were varied to find the minimum fuel consumption for a fixed aircraft and mission. The aircraft modelled is an aircraft of the same size as a Boeing 737-800 and the mission distance is 3700 km. In the comparison the two engine options are assumed to have the same technology level. Results from the study include for example mission fuel consumption, SFC and engine weight.

The tools used were GESTPAN for the mission and engine performance calculations and WEICO for the engine weight calculations. GISMO was used to produce aircraft performance data. After Paper I was written several updates to GESTPAN and WEICO

Table 4.1.1: Polytropic component efficiencies at take-off

	DDTF	GTF
Fan eff [%]	92.4	92.4
Booster/IPC eff [%]	91.8	92.0
HPC eff [%]	92.5	92.5
HPT eff [%]	90.6	91.0
LPT eff [%]	91.0	92.5

have been made, the most important include an updated nacelle model and turbine cooling model. Therefore the study has been repeated and the results are updated within this thesis.

As input to the calculations assumptions on component efficiencies are made. The efficiencies chosen in Paper 1 are repeated in Table 4.1.1. A 0.2 % lower IPC efficiency is assumed for the direct drive engine than the geared. This is because the IPC stage loading is lower for the geared than for the direct drive engine. Since the HPT in the direct drive engine has a slightly higher stage loading due to the higher HPC pressure ratio the efficiency is 0.4 % lower. The efficiency difference between the low pressure turbines has been assumed to be even larger, 1,5 %. The magnitude of the differences are based on trends presented by Grieb [26]

In the presented calculations the engine is designed at take-off conditions i.e. the overall pressure ratio, bypass ratio, inlet Mach numbers etc. are chosen at take-off conditions. This means that for different engine core sizes the over all pressure ratio varies at top of climb despite a constant OPR at take-off.

The overall pressure ratio at take-off conditions is, for the sake of this comparison, assumed to be the same for the two engines. This might not necessarily be true in a full optimization.

4.1.1 Results

In Figure 4.1.1 the relative mission fuel consumption of the two engine configurations is shown as a function of bypass ratio, with the corresponding optimal fan pressure ratio. The optimal bypass ratio for the direct drive configuration is around 13.5. The weight of the engine varies much with varying bypass ratio. This is because the low pressure turbine weight and number of turbine stages changes much with required turbine power. This is a consequence of the low rotational speed and the resulting high stage loading. The optimum bypass ratio for the geared configuration is around 18-19. The fuel consumption with changing bypass ratio is more continuous than for the direct drive. This is because the number of LPT stages do not vary much between the designs. In Table 4.1.2 some performance and weight data of the resulting optimal design for each of the engines is shown.

The low pressure turbine, fan and nacelle are the three heaviest components, and therefore the most important in the trade-off between propulsive efficiency and engine weight. Another important parameter in the trade-off is the nacelle drag. By introducing a gearbox the weight of the LPT can be significantly reduced, and therefore it is possible

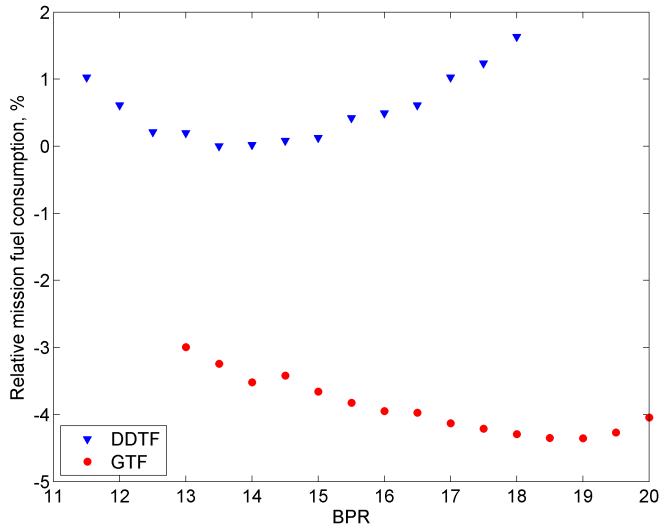

Figure 4.1.1: *Relative mission fuel consumption for the two engine options*

Table 4.1.2: Performance, weight and dimensions of the final configurations. The performance numbers are given for take-off unless stated otherwise

	DDTF	GTF
BPR	13.5	19.0
FPR	1.41	1.3
T3 [K]	902	904
T4 [K]	1850	1850
IPC PR	1.45	2.5
HPC PR	19.6	12.3
OPR	40	40
HPT cooling % of W25	18.0	18.6
Nacelle drag/Total drag, cruise	4.4 %	4.8 %
SFC cruise	base	-4.1 %
Mission fuel consumption	base	-4.4 %
Total engine weight [kg]	3334	3261
Fan diameter [m]	1.9	2.06
Fan weight [kg]	899	1073
LPT weight [kg]	650	211
Nacelle weight [kg]	920	1114

to design the engine with a larger bypass ratio. When comparing the results for the geared turbofan engine presented here to the results presented in Paper I, it can be seen that the LPT weight was not the limiting factor for the geared configuration in the first study. The LPT in the two calculations have approximately the same weight, but the optimal bypass ratio was significantly lower in Paper I than in the updated calculations. As is explained in the next section, the nacelle drag had a larger contribution to total aircraft drag in the earlier calculations. Therefore the nacelle drag was what kept the optimum bypass ratio of the geared engine relatively low.

When comparing the results of the direct drive engine to the results in Paper I, the main difference is that the LPT weight is now substantially higher. The main reason being that GESTPAN now has an updated cooling model to account for the higher cooling mass flow needed for a two stage turbine. This changes the thermodynamic input to the LPT, changing the size and position of the inlet and outlet annulus. For a direct drive engine, the LPT weight is very sensitive to the boundary conditions defined by the inlet and outlet annulus. The reason being that the turbine has a large radius and many stages. The higher cooling flow in the updated calculations leads to a larger core mass flow. The air at the turbine inlet has a lower pressure and density. Thus an increased HPT cooling flow leads to an increased LPT inlet area. Also, a larger enthalpy drop is required over the LPT giving a larger expansion ratio, leading to a larger required outlet area. These differences combined leads to the 17 % heavier turbine in the updated calculations.

The LPT design is very sensitive to how large the turbine is allowed to be radially. The results are therefore very sensitive to how the turbine design constraints are chosen/determined and in practise, how well the turbine can be designed. In this study the efficiency of the LPT does not vary with varying design. When actually designing an LPT, especially for a direct drive engine, trade-off between for example stage loading and efficiency will have to be made.

4.2 Nacelle drag

In Paper I the nacelle drag was approximated as a fixed ratio of total aircraft drag and was scaled with the total wetted area of the nacelle. The baseline nacelle drag amounted to 5 % of the total aircraft drag, but it increased with increasing nacelle diameter. For a BPR 18 geared turbofan engine the total nacelle drag would have been 6 % of the aircraft drag. For the baseline nacelle in these calculations the nacelle drag varies in cruise between 4 and 4.4 % of the total aircraft drag for the direct drive engine, and 4.3-4.8 % for the geared engine. The nacelle drag is a smaller fraction of the aircraft drag at the start of cruise than at the end of cruise.

With the method used in the updated calculations, [27], the nacelle drag coefficient is highly dependent on engine inlet flow conditions. With increasing difference between the far upstream stream tube area and the inlet area ($\frac{A_0}{A_i}$), the drag coefficient of the nacelle increases. For a low thrust setting of the engine the stream tube area is small resulting in a larger drag coefficient.

To test the effect of different nacelle design parameters on nacelle drag, calculations on three different nacelle configurations were made. To study the how the nacelle drag is

affected by the engine design the calculations were done on the geared engine with three different bypass ratios; 12, 15 and 18. The three different nacelle configurations were:

1. Nominal nacelle design
   $L_f/D_{fan} = 0.56$
   $D_m/D_{fan} = 1.207$
   $D_i/D_{fan} = 0.922$
2. Short and ultra thin nacelle
   $L_f/D_{fan} = 0.3$
   $D_m/D_{fan} = 1.05$
   $D_i/D_{fan} = 0.922$
   length factor aft nacelle =0.6
3. Short and medium thin nacelle
   $L_f/D_{fan} = 0.3$
   $D_m/D_{fan} = 1.10$
   $D_i/D_{fan} = 0.922$
   length factor aft nacelle =0.6

In Figure 4.2.1 the nacelle drag and drag coefficient with varying bypass ratio can be seen for the three different nacelle options. Nacelle configuration 1, the nominal nacelle design, has an increasing nacelle drag with increasing bypass ratio. The increase in nacelle drag occurs because the projected frontal area is increasing. The drag coefficient is actually decreasing slightly. For high bypass ratio engines, as the engine core size decreases, the thrust setting in cruise is higher than for a low bypass ratio engine. This means, as the bypass ratio of the engine increases, the difference between the stream tube area and inlet area decreases, resulting in a slightly lower profile drag coefficient. There is no addition to the drag coefficient by spill drag or wave drag. The critical area ratio for this design is 0.56, which is well below, 0.8, the stream tube area ratio for the BPR 12 engine. The drag rise Mach number is approximately 0.86, and it is thus not reached during the mission.

In configuration 2, a very thin and short nacelle design, the critical area ratio is 0.95. The area ratio for the BPR 12 engine is around 0.8 in cruise and for the BPR 18 engine around 0.89. Thus there is spill drag for all three engines. The spill drag is substantially higher for the bypass ratio 12 engine than for the bypass ratio 18 engine. This means that the nacelle drag actually decreases with increasing bypass ratio, despite increasing projected frontal area. Because of the very thin nacelle the drag rise Mach number is well above cruise Mach number, at 0.86-0.87.

To reduce the critical area ratio somewhat compared to the second configuration, the nacelle thickness was increased to 10 % of the fan diameter in the 3rd configuration. This resulted in a critical area ratio of 0.79, just below the area ratio for the BPR 12 engine. The thicker nacelle also resulted in a lower drag rise Mach number of Mach 0.83. This is

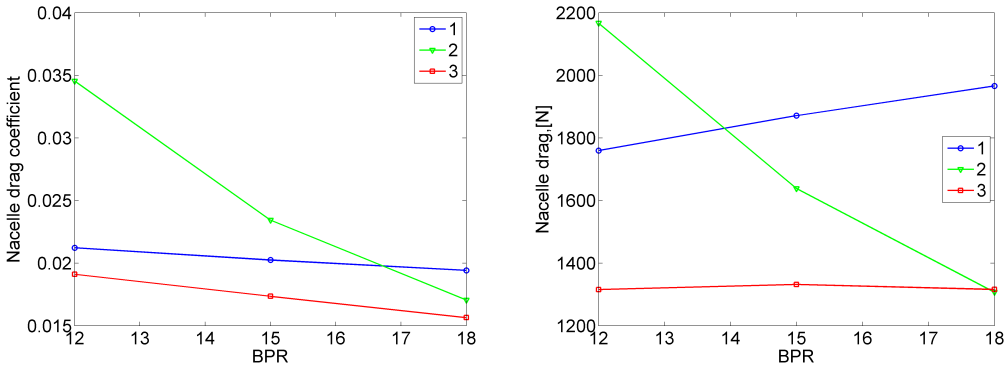

(a) *Nacelle C_D*

(b) *Nacelle drag*

Figure 4.2.1: *Nacelle drag coefficient and nacelle drag for three geared turbofan engines with three different nacelle designs*

below the cruise Mach number in the mission calculated, but the margin is decreased. Results show that the nacelle drag for the 3 different bypass ratios is close to the same for all three configurations. This design turned out to be the best choice giving least nacelle drag for all three chosen bypass ratios, albeit with very little margin. For the BPR 12 engine, only a slight decrease in thrust setting would yield a significant increase in drag due to spill drag. When doing a more in depth study of nacelle design not only the drag for nominal cruise conditions have to be considered, but also other cruise speeds and thrust settings, as well as take-off and climb conditions. Thus it is reasonable to anticipate that the margin to the critical area ratio in design 3 would not be enough for the BPR 12 design. Therefore a high bypass ratio engine might have more margin to the critical area ratio, and thus a thinner nacelle is possible.

The difference in nacelle drag between nacelle design 1 and 3 gives for the BPR 12 engine a 1.4 % decrease in mission fuel consumption, and for the BPR 18 design 1.9 % decrease in fuel consumption.

5 Open rotor

With the open rotor engine concept it is possible to reach higher propulsive efficiency than with a turbofan engine. The majority of the thrust is produced by propellers instead of a fan. Since there is no nacelle shrouding the propellers it is possible to increase propeller diameter and mass flow without increasing nacelle weight and drag.

In Figure 5.0.1 a schematic layout of an open rotor engine is shown. A typical configuration could be one where the core is a two spool turbojet engine consisting of a low pressure compressor (1) followed by a high pressure compressor (2), a combustor (3), high pressure turbine (4) and a low pressure turbine (5). Behind the core there is a power turbine (6) with a shaft to the gearbox (7). The "planets" around the centre wheel are via a carrier connected to one of the propellers (8) and the outer ring of the gear box is connected to the other propeller (9), which rotate in the opposite direction. The exhaust is led in a duct and enters a nozzle after the propellers.

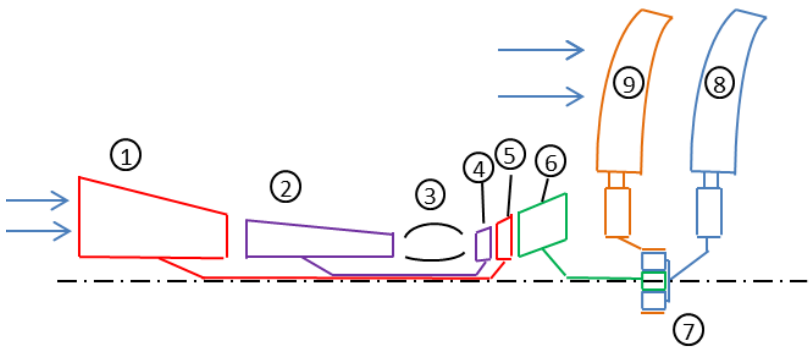

Figure 5.0.1: *Schematic figure of an open rotor engine*

The propeller blades are swept to allow for higher flight speed. The two stage counter-rotating propeller allows for the swirl generated in the first propeller row to be recovered.

The configuration described here is not the only possible configuration. The propellers could for example be placed at the front of the engine or the propellers could be driven by a counter-rotating turbine without a reduction gearbox. The engine can be under wing mounted or fuselage mounted.

Since there is no inlet duct before the propellers the flow conditions will vary substantially between flight speeds. Therefore the propellers need to have variable pitch so that the angle of attack can be changed between different operating conditions. In the case of propellers at the rear of the engine it poses a technical challenge to include a pitch change mechanism that works in the hot exhaust. The control system of the engine is also more complicated than for an ordinary turbofan engine. The turbofan thrust is varied by controlling the fuel flow. In this configuration there is not only the fuel flow to control,

but also two rows of variable pitch propellers.

Admittedly the distinction between a turboprop engine and an open rotor is not very clear. In this thesis an advanced turboprop is defined as a turboprop with a single row of modern swept propeller blades. While an open rotor has swept blades and two counter-rotating propeller rows.

The open rotor concept is not a new one. In the 1980s it was under development and was demonstrated in several flight tests. General Electric together with NASA performed a full scale flight test in a technology demonstrator program called the Unducted Fan (UDF) [35, 36, 37]. This direct driven configuration was flight tested in 1987. At around the same period, Pratt & Whitney together with Allison demonstrated a geared concept called the PW-Allison 578-DX Propfan. This demonstrator flew in 1989. The two previously mentioned concepts never progressed further than flight testing. This is not the case for the Ukrainian/Russian D-27 which powers the Antonov 70 military transport aircraft [38].

5.1 Regional transport application

Today regional aircraft are powered either by turbofan engines or turboprop engines. In the future the open rotor engine might provide an alternative. It would combine the high propulsive efficiency of a turboprop with the turbofans capability of high flight speed. To evaluate the potential of the open rotor engine a comparison of a regional aircraft powered by an open rotor engine, a turbofan engine and an advanced turboprop engine have been made.

The aircraft for which the engines have been evaluated was a 70 passenger aircraft with a range of approximately 3000 km. The aircraft performance, weight and geometry was modelled using GISMO.

The performance of the turbofan and the open rotor engine core was modelled in GasTurb 11. Performance of the counter-rotating propellers was calculated using the method described in Paper II, with the efficiency scaled in accordance with predicted efficiencies presented by Kahlid et al. in [39]. The single propeller was modelled in a similar way, with the propeller performance maps that the counter-rotating maps from Paper II are based on [31]. The efficiency of the single propeller was scaled in accordance with the scaling of the counter-rotating propeller. The weight of the engines is calculated using WEICO.

Details on the comparison between the turbofan and the counter-rotating open rotor can be found in Paper IV. The advanced turboprop was modelled with the same core engine as the open rotor. In Table 5.1.1 the performance data for the three engine options can be seen.

In Figure 5.1.1 the propeller performance maps for Mach 0.75 are shown for both the counter-rotating propeller and the single-rotating propeller. The efficiency shown is the efficiency excluding kinetic losses. The difference between the map for the single-rotating propeller and the counter-rotating propeller is the swirl losses and the scaling of the power coefficient. For the counter-rotating propeller it is possible to reach a higher power coefficient and disc loading due to the two propeller discs. The black markers in the

figure indicate the design point position for the two propellers. The propeller tip speed is chosen to a lower velocity for the counter-rotating propeller. This is possible, as seen in Figure 5.1.1, since the counter-rotating propeller retain a high efficiency with increasing advance ratio.

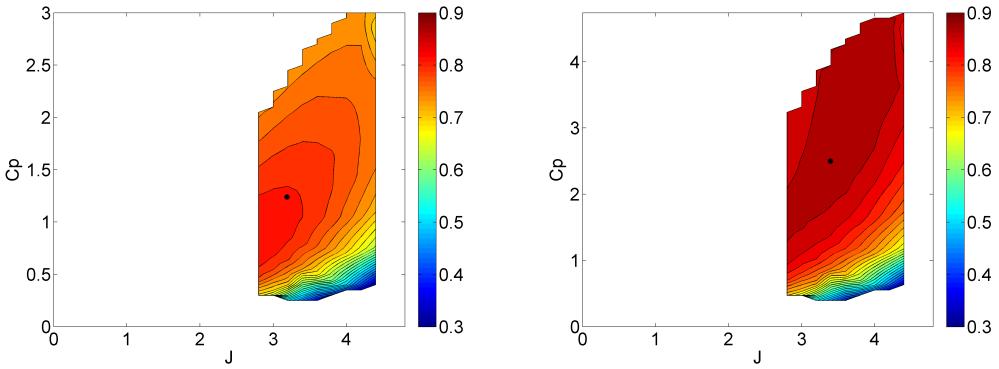

(a) *Advanced turboprop* (b) *Open Rotor*

Figure 5.1.1: *Propeller performance maps at Mach 0.75 for the advanced turboprop and for the open rotor*

Table 5.1.1: Key numbers for baseline engines

	Open Rotor	Advanced TP	Turbofan
Core pressure ratio	25	25	25
Fan pressure ratio	-	-	1.76
Bypass ratio	-	-	8
Propeller disc loading	300 kW/m^2	180 kW/m^2	-
Propeller blade tip speed	214 m/s	228 m/s	-
Burner outlet temperature	1800 K	1800 K	1800 K
Max T41 in cruise	1660 K	1660 K	1660 K
Nozzle pressure ratio, design	1.2	1.2	-
Propeller efficiency	84.5 %	81.5 %	-
Fan polytropic efficiency	-	-	87.5 %
Compressor polytropic efficiencies	88.5 %	88.5 %	88.5 %
HPT polytropic efficiency	88 %	88 %	88 %
LPT polytropic efficiency	87 %	87 %	87 %
Cruise SFC	14.1 g/(kN*s)	14.7 g/(kN*s)	16.0 g/(kN*s)
Propulsion system weight	1460 kg	1380 kg	1150 kg
Propeller /fan diameter	2.77 m	3.69 m	1.09 m

5.1.1 Results

To evaluate aircraft and engine efficiency specific range has been used. This parameter captures the effect of engine performance, aircraft performance as well as weight of the engine and aircraft. In Figure 5.1.2 the specific range for the same aircraft with the three engine options is shown.

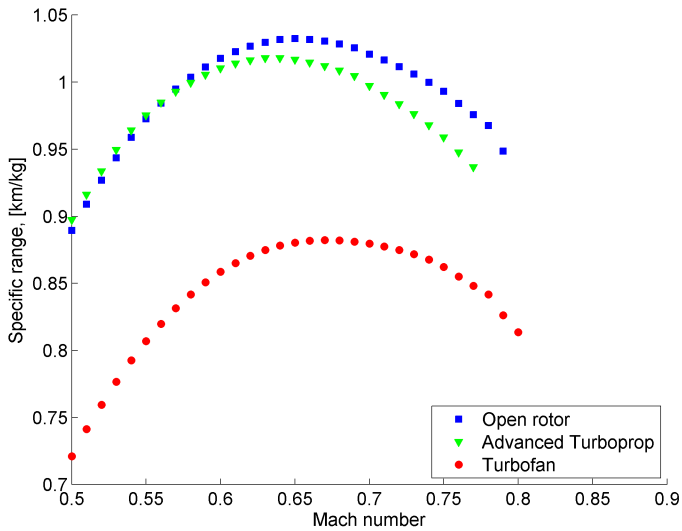

Figure 5.1.2: *Specific range at Flight level 350 for the three studied engine options*

The three engine configurations compared here each have a different long range cruise Mach number. The long range cruise Mach number is defined as the Mach number where the specific range is 99 % of the maximum specific range. For the turbofan this occurs at Mach 0.72, for the open rotor at Mach 0.7 and for the advanced turboprop at Mach 0.68. At maximum specific range the turboprop has a 1.4 % lower specific range than the open rotor, while at Mach 0.77 the difference is 4.0 %. Since the swirl losses increase at higher Mach numbers, there is a larger benefit from counter-rotating propellers at high flight speeds than at low flight speeds. Thus it is not only the swept blades that enable high cruise speeds for an open rotor, it is also an effect of the counter-rotation.

The turbofan engine has a 15.0 % lower specific range than the open rotor at Mach 0.78 and 17.0 % less specific range at long range cruise Mach numbers. The turbofan engine is the configuration that is least sensitive to cruise speed. Thus, there is not as much gain to be had by reducing cruise speed with this configuration as with the open rotor engine or the advanced turboprop engine.

Propeller design point

When changing the design point of the propeller (moving the design point in the map) the efficiency of the counter-rotating propeller and single propeller behave differently. In Figure 5.1.3 the propeller efficiency when not including axial kinetic losses (propeller efficiency divided by propulsive efficiency) for the advanced turboprop and open rotor are shown. The different curves are for different design point propeller disc loadings and tip speeds. As can be seen, for the single propeller the efficiency is rapidly reduced with increasing disc loading. This is because the swirl losses increase as the propeller loading increases. For the counter-rotating propeller where most of the swirl losses are recovered the change in efficiency with propeller loading is much less sensitive. This is also evident when studying the maps in Figure 5.1.1.

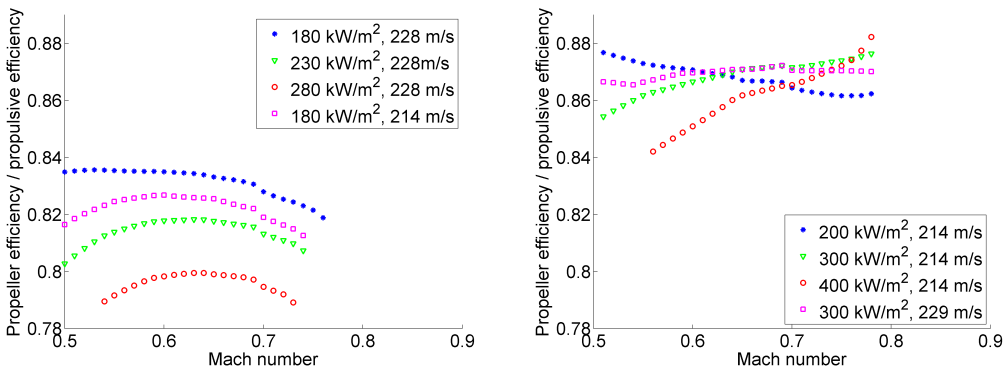

(a) *Advanced turboprop* (b) *Open Rotor*

Figure 5.1.3: *Propeller efficiency/propulsive efficiency for different cruise Mach numbers when changing the propeller design point in the map*

The propulsive efficiency increases with increasing Mach number. In Figure 5.1.4 the propeller efficiency is shown including the axial kinetic losses. With different disc loading the propulsive efficiency of the engine changes. Lower disc loading results in higher propulsive efficiency. For the single propeller this means that the efficiency difference between high and low disc loading is even larger than the differences shown in Figure 5.1.3. Some of the swirl induced losses are cancelled by the increase in propulsive efficiency with higher flight speeds. For the counter-rotating propeller the increase in propulsive efficiency with decreasing disc loading can also favour low disc loading propellers. At least this is the case in terms of high propeller efficiency. However, this benefit is not found in the whole range of Mach numbers, and at high Mach numbers the difference is not very large.

Low disc loading means a larger propeller and a higher weight. Therefore a high propeller efficiency does not necessarily mean a high specific range. In Figure 5.1.5 the variation of specific range with propeller design can be seen for the two propeller options. For the counter-rotating propeller the 300 kW/m^2 disc loading is the best option even though the 200 kW/m^2 disc loading actually has a higher efficiency at most Mach numbers.

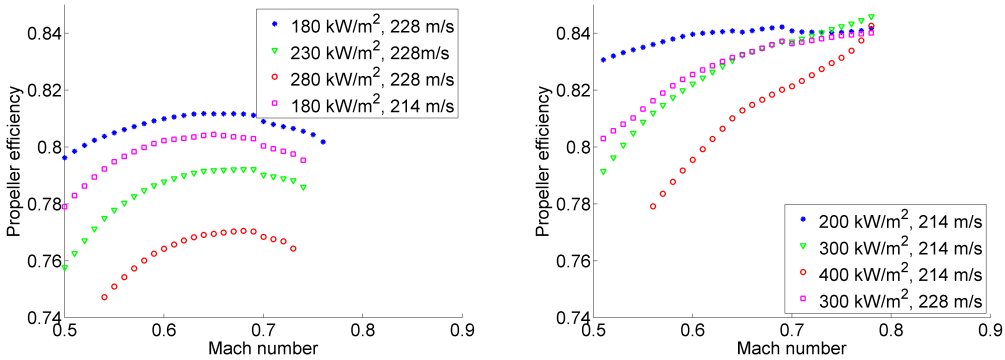

(a) *Advanced turboprop* (b) *Open Rotor*

Figure 5.1.4: *Propeller efficiency for different cruise Mach numbers when changing the propeller design point in the map*

For the single propeller the large differences in propeller efficiency cannot be outweighed by difference in propeller weight. The conclusion is that a single propeller is much more sensitive to choice of disc loading than the counter-rotating propeller. The 180 kW/m^2 propeller design has a propeller diameter of 3.7 m. The counter-rotating propeller design with 300 kW/m^2 disc loading has a diameter of 2.8 m. Still, the single-rotating propeller weighs less than the counter-rotating propellers. Therefore the advanced turboprop engines weighs appropriately 5.6 % less.

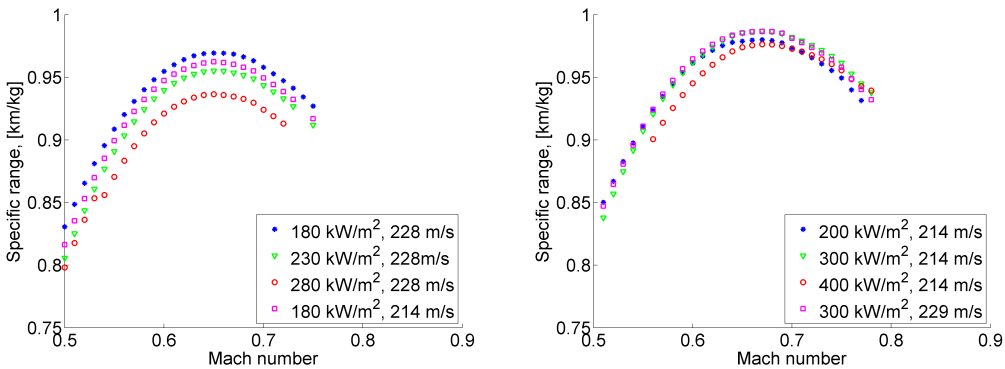

(a) *Advanced turboprop* (b) *Open Rotor*

Figure 5.1.5: *Specific range for different cruise Mach numbers when changing the propeller design point in the map*

Aircraft wing sweep

Relevant when studying the specific range of an aircraft at different Mach numbers is the influence of aircraft wing sweep. In Figure 5.1.6 the specific range and lift over drag for different wing sweep is shown. The aircraft weight is calculated with the same maximum speed in mind.

Lift over drag is for lower Mach numbers fairly alike for the different wing sweep. As the Mach number increases the aircraft efficiency rapidly drops for the lower wing sweep angles. This is because wave drag onset is earlier for lower angles. Wings with less sweep weigh less since the spar is shorter. The combination of the differences in L/D and wing weight shows that 10 degrees wing sweep is most beneficial for Mach numbers below 0.6. 20 degrees sweep is best between approximately Mach 0.6-0.7. Above that a higher wing sweep is needed to avoid compressible drag rise. As is seen, the choice of wing sweep is affected by the design target for the aircraft. If an aircraft is designed to have an as high as possible specific range regardless of Mach number, a wing sweep of around 20 degrees should be chosen. For an aircraft that is designed to have an as efficient operation as possible at Mach 0.78 a 30 degree wing sweep should be chosen.

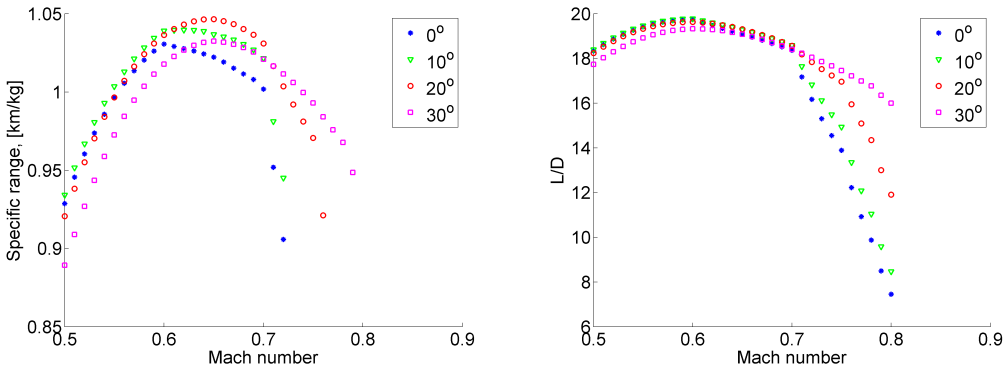

(a) *Specific range* (b) *Lift/Drag*

Figure 5.1.6: *The effect on lift/drag and specific range at different Mach numbers with varying aircraft wing sweep*

The difference in maximum specific range between an aircraft with 20 degrees and with 30 degrees wing sweep is 1.5 %. The difference in weight between these two comparisons is only due to the difference in wing weight. If an aircraft was to be designed with a low wing sweep the intended maximum speed would be lower. Therefore the weight of the aircraft could be lower. In Figure 5.1.2 it can be seen that at low Mach numbers the advanced propfan aircraft actually has a slightly higher specific range than the open rotor aircraft. It is therefore of interest to see how the combination of low wing sweep, lower maximum aircraft speed and an advanced turboprop compares to the high speed open rotor configuration.

In Figure 5.1.7 the baseline open rotor on an aircraft with 30 degree wing sweep and a maximum speed of Mach 0.8, is compared to an aircraft with an advanced turboprop

engine on an aircraft with 10 degrees wing sweep and a maximum speed of Mach 0.72. The change in maximum aircraft speed results in an approximately 500 kg lighter aircraft. The larger part of the difference is difference in wing weight. To withstand flutter an extra weight factor is added for cruise speeds above Mach 0.75. The other large contributors to weight difference is fuselage weight and tail weight. Both these weights are estimated as functions of maximum diving speed [29].

As is seen the specific range at Mach numbers below Mach 0.65 is higher for the turboprop equipped aircraft. The difference in maximum specific range is 0.5 %. At Mach 0.6 the difference is 1.9 %. At Mach 0.72, which is the maximum speed of the turboprop aircraft the difference in specific range is 7.7 %.

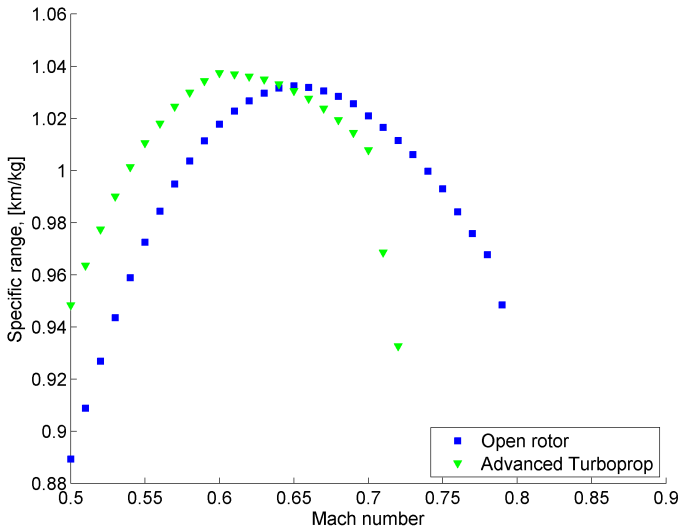

Figure 5.1.7: *Specific range for a regional turboprop aircraft with 10 degree wing sweep and Mach 0.72 maximum cruise speed, compared to the baseline open rotor aircraft configuration*

The choice of the main design parameters for the aircraft and engine is highly dependent on the mission and mix of missions intended for the aircraft. If flight speeds below Mach 0.65 is enough, a turboprop engine will be sufficient. If the possibility of efficient high cruise speed is also desirable then the open rotor option is preferable.

6 Contrail formation avoidance

Reducing the carbon dioxide emissions might not be the only way to lessen the climate effects of aviation. Another way might be to avoid the formation of persistent contrails. Mannstein et al. [40] show that if a region a with RHi greater than 100 % is encountered during flight, in 50 % of the cases it is sufficient to either ascend or descend by 2000 ft in order to exit the ice super saturated region (ISSR) and thus prevent the formation of persistent contrails. If the flight level is changed by 4000 ft then the ISSR can be exited in around 80 % of cases.

In Paper V the change in fuel burn when flying to avoid the creation of persistent contrails is evaluated. Three different avoidance strategies were evaluated with Mannstein et al. [40] as a basis. The strategies are:

Strategy 1: Descend 2000 ft when an ISSR is encountered.

Strategy 2: Ascend 2000 ft when an ISSR is encountered if there is sufficient thrust margin to ascend, otherwise descend 2000 ft.

Strategy 3: Descend 4000 ft when an ISSR is encountered.

In all three cases, the original flight level is resumed if RHi returns to a value below 100 % at the original flight level. It is assumed that the flight crew will have access to on-board humidity measurements as well as some complementary information in order to know when to return to the original flight level. This could, for example, be observations from previous flights on the same route or weather observations and forecasts.

The calculations in Paper V are based on real time humidity data from 81 actual trans-atlantic flights between Frankfurt and Atlanta. The data was collected as a part of the MOZAIC program (Measurement of Ozone and Water Vapor by Airbus InService Aircraft) [41]. The project collects data from in-situ measurements of ozone, water vapour, carbon monoxide, and total nitrogen oxides. The measurements also contain information about true air speed and the current position of the aircraft (latitude, longitude and pressure) and are complimented with meteorological data (wind speed and direction and static air temperature). The data was collected by sensors on-board six Airbus A340 aircraft, which operate for European commercial airlines. The data was automatically collected at intervals of approximately four seconds (roughly equivalent to every 1 km) during round-trip international flights.

6.1 Modelling

The measurements and calculations were based on the A340-300 aircraft equipped with four CFM56-5C engines. The aircraft lift and drag for different angle of attack and Mach numbers were calculated using GISMO. Much of the key information required to model the aircraft performance is available in the public domain [42]. Since these calculations were limited to cruise conditions, the Reynolds number effect on aircraft performance due to variations in altitude is assumed to be negligible.

The engine thrust and SFC for different operating conditions were calculated using GasTurb 11. Input to the engine performance calculations have been collected from openly available data [38, 43].

Using the method described in Section 3.6, the fuel consumption for the cruise part of the flown mission was calculated. Thereafter the fuel consumption for the new flight trajectories according to the three evaluated avoidance strategies was calculated.

Since it is the effect of changing altitude that is sought, it is important to know how well the models can predict at what aircraft mass a climb should be attempted in order to minimize fuel burn. As an aircraft burns fuel and the aircraft weight is reduced the optimal cruise altitude increases. For long flights, cruise altitude is increased in steps as the mass of the aircraft decreases. For each such step there is an aircraft weight for which the fuel consumption starts being lower at the higher altitude than at the lower altitude. This can be seen in Figure 6.1.1a, where the one curve represents the fuel consumption at the lower altitude and the other at higher altitude. The intersection between the curves indicate optimal climb mass. What the optimal mass is varies with Mach number, ambient temperature and altitude.

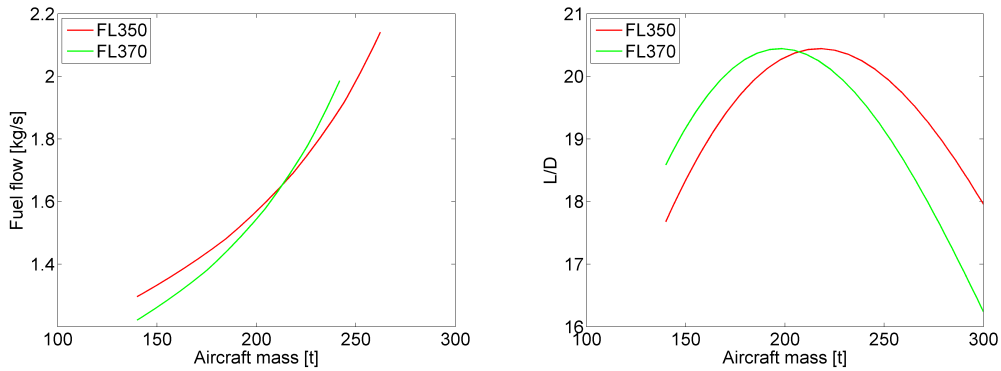

(a) *Engine fuel flow* (b) *Lift over drag*

Figure 6.1.1: *Engine fuel flow and lift over drag at different aircraft mass for two different flight levels*

The main parameter affecting the location of the optimum is at what C_L the maximal ratio between C_L and C_D occur. In Figure 6.1.1b L/D for two different altitudes is plotted for a range of aircraft weights. The intersection between the two curves roughly represents the weight for which an optimal climb can be made, but not entirely since there is an effect from engine performance as well. It is clearly seen that if the position of the maximum L/D is moved, so is the resulting optimum mass for a climb. In the aircraft performance modelling this is largely governed by the so called blade technology factor [4]. This factor govern at what Mach number the wave drag due to transonic conditions occur. If the technology factor is high the onset of wave drag is delayed to higher angles of attack for a given Mach number and the maximum value of L/D is moved towards a higher C_L. To test how different technology factors affect the results the magnitude of the factor

was varied. As an example based on the curves in Figure 6.1.1, with a climb from FL350 to FL370 at Mach 0.8, the optimum climb weight is moved 2400 kg between the lowest and highest technology factor tested. That corresponds to approximately 24 minutes difference in when it is best to climb. The effect of climbing 24 minutes too early or too late with respect to optimum, results in less than 4 kg of extra fuel burn. Therefore the models are judged to be accurate enough to capture the sought effects.

The second important modelling uncertainty to look at is the weight of the aircraft at the start of cruise. Within the MOZAIC data no information on aircraft weight is included. Thus it is necessary to approximate what the mass at start of cruise was in each of the missions. Even though the same city pair has been evaluated, the same amount of fuel will not have been carried every time. The payload varies with each mission and the planned route varies between missions. To assume the same initial weight for all missions would completely skew the results.

The aircraft weight when cruise is commenced is approximated for each individual mission by looking at how lift/drag varies over the mission, particularly within the last phase. In the ideal case the maximum value of L/D for each flight level would occur around the middle of each phase. Of course this rarely the case. It is relatively certain that the last climb is not made to end up at an altitude higher than the optimal altitude for that weight. Thus it can quite safely be assumed that L/D at some point is at its maximum within the last phase, or possibly that the aircraft is on the lighter side of the optimum. Otherwise, no climb would have been attempted. An initial mass for start of cruise between is chosen between 210 and 240 tons for each mission. The initial guess is then adjusted if judged necessary by visual inspection of the L/D-curves. Of course it is still not possible to be entirely sure if the approximated aircraft weight is correct. The same calculations have therefore been carried out with 5 tones more and 5 tones less fuel than for the baseline mission. For the individual mission this can make some difference in the resulting change in fuel burn, but over all the numbers stay quite near the baseline.

6.2 Results

The calculations show that when using Strategy 1, 2000 ft descent, the fuel consumption is on average increased by 0.4 % and when using Strategy 3, 4000 ft descent, the fuel consumption is increased by 1.2 %. Calculations using Strategy 2, 2000 ft ascent, show no significant difference in the annual fuel consumption. The change in fuel consumption is not the same for all missions. In Figure 6.2.1 the change in fuel consumption for the individual missions are shown for the 2000 ft ascent and descent strategies. When Strategy 1 is used a majority of the individual missions show an increase in fuel consumption whilst some show no change. In contrast, when Strategy 2 is used approximately half of the flights show a reduced fuel burn. Strategy 3, although not shown here, displays the same trends as Strategy 1, only with larger changes.

As is evident from the Strategy 2 results, in approximately half of the missions the optimal altitude was at a higher altitude than flown, since approximately half of the flight level increases resulted in a fuel consumption decrease.

In Figure 6.2.2, the altitude profiles are shown for three selected missions denoted A,

(a) *Strategy 1, Descend 2000 ft* (b) *Strategy 2, Ascend 2000 ft*

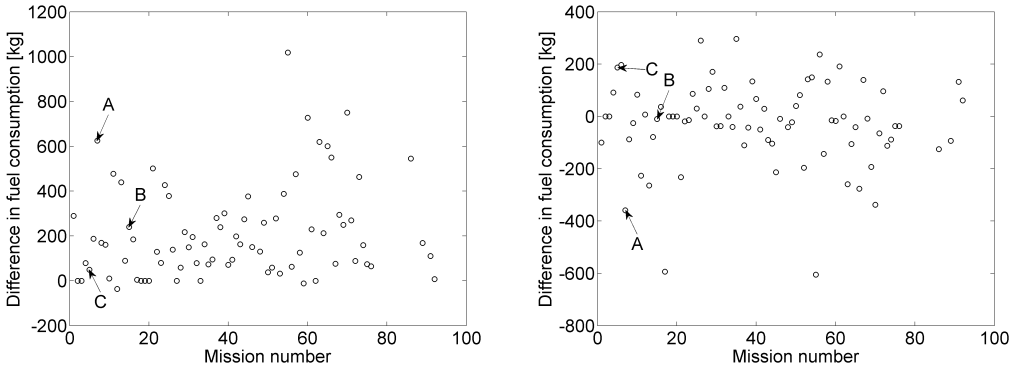

Figure 6.2.1: *Resulting change in fuel consumption for the individual missions from Frankfurt to Atlanta when using Strategy 1 (2000 ft descent) to the left and Strategy 2 (2000 ft ascent) to the right. A, B and C refer to the three missions shown in Figure 6.2.2.*

B and C, using Strategy 1 (to the left) and Strategy 2 (to the right). These missions are also indicated in Figure 6.2.1. Mission A shows a flight where an extended period was spent at a lower than optimal altitude. Contrail avoidance Strategy 1, where the altitude was reduced and the aircraft ended up even further from the optimum altitude, resulted in a significant increase in fuel consumption. Strategy 2, on the other hand, for which the altitude was increased shows a decrease in mission fuel consumption. It can be noted that the decrease when using Strategy 2 is not as large as the increase when using Strategy 1 despite the fact that the absolute change in altitude is the same. This is because the effect of non-optimality is greater the further from optimal altitude the aircraft is flying.

In mission B the ISSR region is at a flight level close to, but slightly below, optimum flight altitude. An indication of what the optimal flight level would be can be deduced from Figure 6.2.1. When changing altitude according to Strategy 2 there is no significant change in fuel consumption, thus the optimum flight level for that region is in between the original and the new flight level. A descent by 2000 ft (Strategy 1) yields a fuel burn increase, but the increase is less than in mission A, partly because the new altitude is still fairly close to the optimal altitude.

In mission C the original altitude during flight through the contrail risk regions was also close to optimal. In this case there was an increase in fuel consumption when ascending to a higher altitude (Strategy 2) and no significant change when descending (Strategy 1).

It is evident that real transatlantic missions are often flown at non-optimal altitudes. If part of a mission is flown at an altitude far from the optimal, any changes made to the altitude results in large changes in fuel consumption. If the altitude is close to optimal then small changes in altitude have little effect on the fuel consumption. For the same reason a 4000 ft change in altitude yields on average a fuel penalty that is three times larger than a 2000 ft change. Therefore, airlines which adopt a "green flight" policy

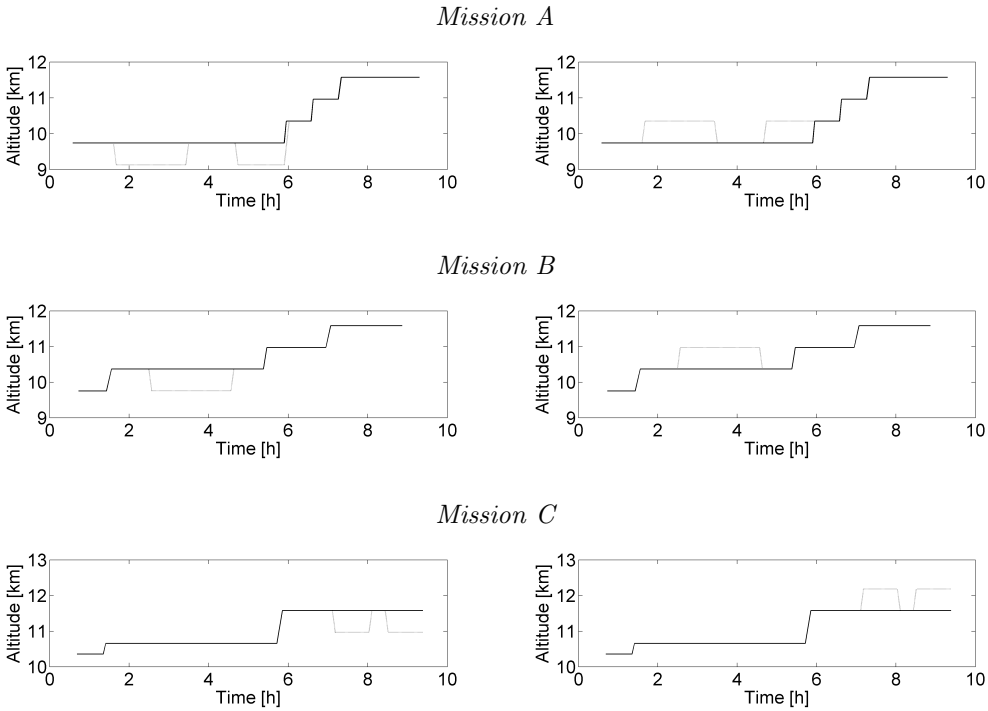

Figure 6.2.2: *Cruise profiles for the three missions indicated in Figure 6.2.1. The solid line represents the cruise profile of the flight. The dashed line represents the alternative profile to avoid ISSRs. Strategy 1 to the left and Strategy 2 to the right.*

with the aim of flying close to the fuel-optimal altitude will only carry a very small fuel consumption penalty, whilst airlines that regularly select an altitude further from the optimal will suffer a larger penalty. If it is assumed that there will be more flexibility for an airline to choose an optimal altitude in the future, the penalty for the 2000 ft descent strategy will be even less than the 0.4 % penalty presented here.

6.3 Comparison to other studies

There have been many suggestions put forward on how to operate aircraft to reduce the climatic impact from contrail formation. One of the most complete approaches to minimizing the aviation induced radiative forcing has been explored by Matthes et al. [44]. The paper takes the effects of carbon dioxide emissions, NO_x, water vapour and contrail formation into account when doing route optimization. They show that by using weather predictions to calculate the radiative forcing of a contrail over its lifetime it is possible to optimize the route for minimal radiative forcing. Although this approach has the potential to significantly reduce the climatic impact of a flight, it requires access to a large number

of models concerning the climatic impact of different emissions as well as meteorological predictions. The benefit of the avoidance method studied herein is that very little change is required to existing ATM procedures [45]; procedures for route planning and requests for altitude changes would remain the same as in current operations, although requests would be made more frequently.

Other suggestions have been put forward on, for example, introducing an operational ceiling for air traffic to minimise the risk of flying through a region where persistent contrails might form [46, 47]. The drawback with this approach is that a low operational ceiling increases airspace congestion, thus increasing the workload for air traffic controllers. They also show that the fuel burn penalty for imposing an operational ceiling between 24 and 31 thousand feet is on average 3.9 % over the entire year. That means almost a tenfold increase compared to the 2000 ft descent strategy presented here.

Other attempts at evaluating the fuel burn penalty for a contrail avoidance similar to the ones described here have been made. Schwartz et al. [48] has made similar calculations to see the fuel burn penalty when deviating from the optimal mission profile for 20 % of the flight distance. Used in their mission calculations was the Boeing Mission Analysis Program, where aircraft specific information is included. Since the calculations in Paper V were made using real mission profiles and actual measured humidity data the results slightly differ from the idealized calculations by Schwartz et al. Their results show a 0.2 - 0.7 % increase in block fuel consumption, whereas the calculations in Paper V show a 0.0 - 1.2 % change in cruise fuel consumption. The major reason for these differences is the frequent lower than optimal flight altitudes in the real flights.

Schumann et al. [49] have evaluated the potential to reduce the climate impact of aviation by changing the flight level. Their calculations include an estimate on fuel consumption change for 2000 ft ascent or descent. Their method to calculate the change in fuel consumption included generalized trends on how the fuel consumption for an aircraft fleet changes with changing altitude. Thus, no calculations for how the fuel consumption for an individual aircraft changes is made. Their trends show a decreasing fuel consumption with an increasing altitude, and an increasing fuel consumption for a decreasing altitude (1 % change in fuel flow for 2000 ft change in altitude). Thus the fact that there is an optimal flight altitude that varies with weight is missed.

7 Comments to papers

7.1 Paper I

In Paper I the mission fuel consumption of a geared turbofan have been compared to the fuel consumption of a two shaft direct drive turbofan. The engines are compared for the same technology level. Different assumptions on efficiencies have been made to account for the inherent differences between the two architectures. The main part of the calculations have been carried out by this author with support from the co-authors. The aircraft performance was at an earlier date modelled by the second author Richard Avellán.

In Chapter 4 this comparison has been discussed and the calculations have been updated with use of refined models of certain components.

7.2 Paper II

The open rotor engine is one of the most discussed and a promising options to reach low fuel consumption. In order to independently value the open rotor concept it is important that methods to model the performance of counter-rotating propellers are available in the public domain.

In Paper II an extensive propeller performance map available within the public domain has been used as a basis to create a map that captures the general performance of counter-rotating propellers. The difference in performance characteristics between a single-rotating and a counter-rotating propeller is visualised. The propeller representation is simple and can readily be implemented into standard gas turbine performance tools.

The main part of the calculations have been carried out by this author with support from the co-authors.

7.3 Paper III

Paper III covers some radical concepts for propulsion installation for commercial aircraft. The concepts covered are shape changing nacelle, deployable noise shielding nacelle, and deployable propulsor. It is the authors' hope that this paper will inspire studies of more radical propulsion integration concepts in the future.

The main part of the work has been done by the first author of the paper, Anders Lundbladh. This authors contribution to the paper is the mission fuel consumption calculations of the noise shielded open rotor and the mission fuel consumption calculations of an high bypass ratio turbofan engine with an ultra-short and thin nacelle.

Related to this an additional nacelle study is included in Section 4.2.

7.4 Paper IV

Today many of the routes between small to medium sized airports and large hubs are operated by regional aircraft. Current regional aircraft are powered by turboprop or turbofan engines. In the future the open rotor engine might provide an alternative. Therefore it is of interest to evaluate the potential of the open rotor engine within this market segment.

In Paper IV a regional aircraft equipped with either turbofan engines or open rotor engines have been compared in terms of aircraft specific range. How the specific range of the two concepts vary with varying Mach numbers and design choices have been analysed. This comparison is discussed in Chapter 5 where also an analysis of an advanced turboprop is included.

The main part of the calculations have been carried out by this author with support from the co-authors.

7.5 Paper V

Since persistent contrails and contrail induced cirrus clouds have an effect on the climate it might be of interest to fly so that the creation of persistent contrails is decreased. In Paper V the change in fuel consumption when utilising a contrail avoidance scheme is calculated. The calculations are based on real flight and humidity data for 81 transatlantic flights. The results are presented in Chapter 6 together with an analysis of model uncertainties.

The fuel consumption calculations and aircraft/engine modelling was performed by this author. The bulk of the measurement data analysis and processing was made by the second author Deborah Mitchell.

8 Conclusions

Different concepts to reduce the environmental impact of aviation have in this work been analysed and evaluated. The main part of the work deals with high propulsive efficiency engines. Historically there has been a trend towards increased propulsive efficiency for turbofan engines. The next step in this direction is the geared turbofan engine. Engines of this type will enter service in the coming years. Beyond this there is the open rotor option, which has the potential to significantly improve propulsive efficiency compared to the turbofan engines under current development. It should be noted that in order to minimise engine fuel consumption, increased propulsive efficiency is not enough. The concepts studied here will have to be combined with cycles that also increase thermal efficiency.

In the analysis of future aircraft and engine options, a range of conceptual design tools have been used. These studies enable the benefits and limitations of the different concepts to be evaluated. The concepts and design choices can be analysed without having access to detailed design data. This allows for independent and transparent evaluations. Note that the results are dependent on if the envisioned component efficiencies and technology levels will be reached. These results do not reflect the performance of specific future engines, they rather show the relative merits of different concepts and the effect of design trade-offs that might be necessary.

It was seen that the geared turbofan has the possibility to reach approximately 4 % lower mission fuel consumption compared to a two shaft direct drive turbofan. The largest benefits of the geared engine compared to the direct drive engine, is the significantly lower LPT weight. The higher rotational speed of the geared LPT results in fewer stages and thus fewer parts, which is also beneficial from a cost perspective.

It was found that the fuel consumption results of the direct drive engine is very sensitive to the geometrical constraints of the LPT. Small changes in for example radial extension of the turbine lead to large differences in weight. In the actual design of such an engine there needs to be a trade-off between component efficiency and weight.

In the analysis of the geared configuration it was found that the nacelle drag might limit the achievable propulsive efficiency. When reducing the nacelle drag from approximately 5-6 % to 4-5 % of the total aircraft drag the resulting optimal bypass ratio of the geared turbofan was significantly increased. No such effect was found for the direct drive engine since the LPT weight is a greater limitation.

The comparison of a regional open rotor aircraft and an advanced turboprop aircraft show that the counter-rotating propeller configuration will maintain higher efficiency at high cruise Mach numbers than the single propeller stage. This is because the swirl losses of the single propeller increase with the increasing power requirements.

What the right design choices are regarding for example wing sweep angle, single or counter-rotating propeller, maximum design speed and so on depends on the market requirements for the aircraft. For the regional aircraft configuration shown in this thesis, if a cruise speed below Mach 0.65 is desired a single-rotating propeller on an aircraft with 10 degrees wing sweep is adequate. If cruise speeds up to Mach 0.8 is required, 30 degrees wing sweep and a counter-rotating propeller is preferable. Other design requirements

might come to play a role in the dimensioning, such as landing weight, intended runway length, climb gradient and so on.

As is discussed in the introduction, it is not always evident what trade-offs should be made in order to reduce the climate impact of aviation. When comparing contrail formation to CO_2 emissions it is not evident what the optimal trade-off is. CO_2 has a residence time in the atmosphere in the order of centuries, while persistent contrails disappear within hours or days. On the other hand, the local radiative forcing of contrails is large and in certain regions there is more or less constant air traffic. In such regions old contrails do not have time to disappear before new are formed. To fully evaluate the potential gain from implementing an avoidance strategy, a trade-off study between the climate effects from CO_2 emissions and contrail formation is needed.

In the analysis of how contrail formation avoidance would affect fuel consumption for real transatlantic flights, it was found that aircraft often fly at lower than optimal altitudes. This has an effect on the change in fuel consumption when avoiding contrail formation. Aircraft at optimal flight altitudes will have a lower penalty than flights that start out at non-optimal altitudes.

8.1 Future work

When studying future engine concepts, refinement of the models used needs to be made in parallel with the development of the concepts and increased availability of public engine data. The refinement should start with those components that have a large impact on the overall fuel consumption. Below some suggestions for further improvements to calculations presented in this thesis are given.

For the direct drive turbofan engine it would be beneficial to do a mechanical and aerodynamic layout of the low pressure turbine so that a trade-off between efficiency and turbine weight can be made. For the low pressure turbine this is relevant since its weight account for a large portion of the engine weight.

To maximise the potential of turbofan engines the nacelle drag needs to be minimised. In this thesis the nacelle drag studies are based on methods applicable to relatively conventional nacelle configurations. If significant progress is going to be achieved, more detailed studies of low drag installation concepts are needed.

Since the open rotor engine is a concept that has not yet reached commercial operation, the publicly available data needed to refine the propeller performance and weight models is limited. As more and more data becomes available it will be possible to validate and improve the propeller performance modelling against state of the art propeller designs. In the current models, up to date propeller performance data for static conditions are lacking, therefore the models do not allow for runway length optimisation etc.

To improve the weight modelling of the propeller module and to reduce the uncertainties to a level on a par with conventional turbofan engines, additional mechanical and rotor dynamical analysis is needed.

The study of the regional open rotor is an early study on the effect of the propulsion system on the cruise energy efficiency. The next step would be to use the knowledge gained within this thesis as a basis to do an optimisation study.

Bibliography

[1] A. Schäfer, "Long-term trends in global passenger mobility," *The Bridge*, vol. 36, no. 4, pp. 24–32, 2006.

[2] "ICAO International Civil Aviation Organization, Annual reports of the council." http://www.icao.int/publications/Pages/annual-reports.aspx, 2013.

[3] "gapminder.org," 2013. Last accesed: 2013.12.01.

[4] R. Avellán, *On the Design of Energy Efficient Aero Engines: Some Recent Innovations*. PhD thesis, Chalmers University of Technology, 2011.

[5] "International energy agency."

[6] R. Sausen, I. Isaksen, V. Grewe, D. Hauglustaine, D. Lee, G. Myhre, M. Köhler, G. Pitari, U. Schumann, F. Stordal, and C. Zerefos, "Aviation radiative forcing in 2000: An update on IPCC (1999)," *Meteorologische Zeitschrift*, vol. 14, no. 4, pp. 555–561, 2005.

[7] U. Schumann, "Formation, properties and climatic effects of contrails," *Comptes Rendus Physique*, vol. 6, 2005.

[8] P. Minnis, J. Ayers, R. Palikonda, and D. Phan, "Contrails, cirrus trends, and climate," *Journal of Climate*, vol. 17, no. 8, pp. 1671–1685, 2004.

[9] J. E. Penner, D. H. Lister, D. J. Griggs, D. J. Dokken, and M. McFarland, "IPCC special report, aviation and the global atmosphere," *IPCC, Intergovernmental Panel on Climate Change*, 1999.

[10] D. Lee, G. Pitari, V. Grewe, K. Gierens, J. Penner, A. Petzold, M. Prather, U. Schumann, A. Bais, T. Berntsen, D. Iachetti, L. Lim, and R. Sausen, "Transport impacts on atmosphere and climate: Aviation," *Atmospheric Environment*, vol. 44, no. 37, pp. 4678–4734, 2010.

[11] C.-C. Chen and A. Gettelman, "Simulated radiative forcing from contrails and contrail cirrus," *Atmospheric Chemistry and Physics Discussions*, vol. 13, no. 4, pp. 10939–10959, 2013.

[12] A. Karyd, "Fossilfri flygtrafik?." Underlagsrapport till utredningen om fossiloberoende fordonsflotta, N 2012:05, oct 2013.

[13] "The EU Emissions Trading System (EU ETS)." http://ec.europa.eu/clima/policies/ets/index_en.htm, jan 2014.

[14] "Dramatic MBM agreement and solid global plan endorsements help deliver landmark ICAO 38th assembly." http://www.icao.int/Newsroom/Pages/mbm-agreement-solid-global-plan-endoresements.aspx, oct 2013.

[15] "Aviation emissions: Commission proposes applying EU ETS to european regional airspace from 1 january 2014." http://europa.eu/rapid/press-release_MEMO-13-906_en.htm, oct 2013.

[16] "Reducing emissions from aviation." http://ec.europa.eu/clima/policies/transport/aviation/, jan 2014.

[17] J. Meltzer, "The international civil aviation organizations regulation of CO_2 emissions: Amending the EU aviation directive to avoid a trade war," oct 2013.

[18] N. Dickson, "Progress on the development of the icao co_2 standard," May 2013.

[19] J. Kurzke, "GasTurb 11, user manual," 2007.

[20] T. Grönstedt, *Development of methods for analysis and optimization of complex jet engine systems*. PhD thesis, Chalmers University of Technology, 2000.

[21] J. Young, R. Wilcock, and H. JH, "Modeling the air-cooled gas turbine: Part 2-coolant flows and losses. discussion," *Journal of turbomachinery*, vol. 124, no. 2, pp. 214–222, 2002.

[22] R. Wilcock, J. Young, and J. Horlock, "The effect of turbine blade cooling on the cycle efficiency of gas turbine power cycles," *Journal of engineering for gas turbines and power*, vol. 127, no. 1, pp. 109–120, 2005.

[23] K. G. Kyprianidis, D. Au, S. O. Ogaji, and T. Grönstedt, "Low pressure system component advancements and ist impact on future turbofan engine emissions," *ISABE 2009-1276*, 2009.

[24] L. Larsson, T. Grönstedt, and K. G. Kyprianidis, "Conceptual Design and Mission Analysis for a Geared Turbofan and an Open Rotor Configuration," *Proceedings of ASME Turbo Expo 2013: Turbine Technical Conference and Exposition*, no. GT2011-46451, 2011.

[25] E. Onat and G. W. Klees, "A method to estimate weight and dimensions of large and small gas turbine engines," *NASA-CR-159481*, 1979.

[26] H. Grieb, *Projektierung Von Turboflugtriebwerken*. Birkhauser, 2004.

[27] ESDU, "Drag of axisymertic cowls at zero incidence for subsonic Mach numbers," tech. rep., 1981.

[28] R. Avellán and T. Grönstedt, "Preliminary design of subsonic transport aircraft engines," *ISABE 2007-1195*, 2007.

[29] E. Torenbeek, *Synthesis of subsonic airplane design: an introduction to the preliminary design of subsonic general aviation and transport aircraft, with emphasis on layout, aerodynamic design, propulsion and performance*. Springer, 1982.

[30] J. Roskam, *Airplane Design Part VI: Preliminary Calculation of Aerodynamic, Thrust and Power Characeristics*. 2004.

[31] J. Baum, P. Dumais, M. Mayo, F. Metzger, A. Shenkman, and G. Walker, "Prop-fan data support study," *NASA-CR-152141*, 1978.

[32] J. B. Delano and J. L. Crigler, "Compressible-flow solutions for the actuator disk," *NACA RM L53A07*, 1953.

[33] G. Hoff, "Experimental performance and acoustic investigation of modern, counter-rotating blade concepts," *NASA Contractor Report 185158*, 1990.

[34] A. Guha, "Optimum fan pressure ratio for bypass engines with separate or mixed exhaust streams," *Journal of Propulsion and Power*, vol. 17, no. 5, pp. 1117–1122, 2001.

[35] "Full scale technology demonstration of a modern counterrotating unducted fan engine concept, engine test," Tech. Rep. NASA CR-180869, NASA, 1987.

[36] "Full scale technology demonstration of a modern counterrotating unducted fan engine concept, design report," Tech. Rep. NASA CR-180867, NASA, 1987.

[37] C. Reid, "Overview of flight testing of GE aircraft engines UDF engine," No. AIAA-88-3082 in 24th joint propulsion conference, (Massachusetts), AIAA/ASME/SAE/ASEE, 1988.

[38] M. Daly and B. Gunston, "Janes aero-engines," 2010.

[39] S. A. Khalid, J. P. Wojno, A. Breeze-Stringfellow, D. P. Lurie, T. H. Wood, K. Ramakrishnan, and U. Paliath, "Open rotor designs for low noise and high efficiency," *Proceedings of ASME Turbo Expo 2013: Turbine Technical Conference and Exposition*, no. GT2013-94736, 2013.

[40] H. Mannstein, P. Spichtinger, and K. Gierens, "A note on how to avoid contrail cirrus," *Transportation Research Part D: Transport and Environment*, vol. 10, no. 5, pp. 421–426, 2005.

[41] A. Marenco, V. Thouret, P. Nédélec, H. Smit, M. Helten, D. Kley, F. Karcher, P. Simon, K. Law, J. Pyle, *et al.*, "Measurement of ozone and water vapor by airbus in-service aircraft: The mozaic airborne program, an overview," *Journal of Geophysical Research*, vol. 103, no. D19, pp. 25631–25, 1998.

[42] Airbus, "A340-300 specifications." http://www.airbus.com/aircraftfamilies/passengeraircraft/a340family/a340-300/specifications/, 2013. Last accessed 2013.10.17.

[43] CFMI, "CFM56-5C turbofan engine." http://www.cfmaeroengines.com/engines/cfm56-5c, 2013. Last accessed 2013.10.17.

[44] S. Matthes, U. Schumann, V. Grewe, C. Frömming, K. Dahlmann, A. Koch, and H. Mannstein, "Climate optimized air transport," in *Atmospheric Physics*, pp. 727–746, Springer, 2012.

[45] ICAO, "Guidance concerning air navigation in and above the north atlantic MNPS airspace." NAT Doc 007, 2011.

[46] V. Williams, R. B. Noland, and R. Toumi, "Reducing the climate change impacts of aviation by restricting cruise altitudes," *Transportation Research Part D: Transport and Environment*, vol. 7, no. 6, pp. 451–464, 2002.

[47] V. Williams and R. B. Noland, "Variability of contrail formation conditions and the implications for policies to reduce the climate impacts of aviation," *Transportation Research Part D: Transport and Environment*, vol. 10, no. 4, pp. 269–280, 2005.

[48] E. Schwartz, S. L. Baughcum, and D. L. Daggett, "Quantifying the fuel consumption penalties for an operational contrail avoidance system," *SAE Technical Paper 01-3151.*, vol. 2009.

[49] U. Schumann, K. Graf, and H. Mannstein, "Potential to reduce the climate impact of aviation by flight level changes," in *3rd AIAA Atmospheric and Space Environments Conference, AIAA paper*, vol. 3376, pp. 1–22, 2011.